Supporting Information for

Distal Conformational Locks Guide Reaction Pathways for Enhanced Metallocene Mechanochemistry

Yudi Zhang,[1] Zi Wang,[1] Tatiana B. Kouznetsova,[1] Ye Sha,[2,3] Enhua Xu,[4] Logan Shannahan,[5] Muge Fermen-Coker,[5] Chuanbing Tang,[2,*] Stephen L. Craig[1,*]

[1]Department of Chemistry, Duke University, Durham, North Carolina 27708, United States
[2]Department of Chemistry and Biochemistry, University of South Carolina, Columbia, South Carolina 29208, United States
[3]College of Science, Nanjing Forestry University, Nanjing, 210037, China
[4]Graduate School of System Informatics, Kobe University, Kobe 657-8501, Japan
[5]US Army Research Laboratory, Maryland MD 21005, United States

Table of Contents

1. General Experimental Details

1.1 Materials

Ferrocene (98%), $LiAlH_4$ (95%), $AlCl_3$ (99%), n-BuLi solution (1.6M, in hexanes), potassium tert-butoxide (> 98%), 3-buten-1-ol (96%), N-(3-Dimethylaminopropyl)-N′-ethylcarbodiimide hydrochloride (EDCl, 98%), dimethylaminopyridine (DMAP, 98%), ethyl vinyl ether (EVE, 99%), Grubbs II catalysts (98%), 2,4,6-Tris(2-pyridyl)-*s*-triazine and 1,10-phenanthroline were purchased from Sigma-Aldrich and used as received. Acryloyl chloride (97%) and 9-oxabicyclo[6.1.0]non-4-ene (epoxy COD, 95%) was purchased from Sigma-Aldrich and freshly distilled before use. CO_2 (99.999%) was purchased from Airgas. [3]ferrocenophane and [5]ferrocenophane was synthesized according to literature.[1,2] All solvents were dried unless otherwise stated.

1.2 Characterization and methods

^1H NMR and ^{13}C NMR spectra were recorded on a 400 MHz or 500 MHz Varian NMR spectrometer sing $CDCl_3$. The chemical shifts are reported with respect to $CHCl_3/CDCl_3$(δ(1H) =7.26 ppm, δ(13C) =77.0 ppm). ESI-MS spectra were collected on an Agilent LC/MSD Trap instrument.

1.3 SMFS Measurements

Details regarding the instrumentation, data acquisition, and experimental parameters are identical to those conducted previously by our group, except that the solvent employed here was toluene. All experiments were performed at ambient temperature (~23 °C) using a homemade Atomic Force Microscopes, which are constructed of a Digital Instruments scanning head mounted on top of a piezoelectric positioner. Cantilever Probes with spring constants in the range of 20-30pN/nm: Sharp Microlever silicon probes (MSNL), and Silicon Nitride AFM probes (PNP-DB) were purchased from Bruker (Camarillo, CA) and NanoAndMore USA Corp (Watsonville, CA) correspondingly. The spring constants were calibrated for each probe in air, using methods described previously. Force curves were collected on dSPACE (dSPACE Inc. Wixom, MI) and National Instruments (Austin, TX) hardware and analyzed using Matlab (The MathWorks, Inc., Natick, MA). All data were filtered during acquisition at 500 Hz. After acquisition, the data were processed and plotted plotted by using homemade software written in Matlab. Force-clamp experiments were performed according to procedures previously reported by our group.[3]

1.4 Force-clamping experiments

For the force clamp experiments data were collected in a similar automated grid pattern, with exception that when the experimental apparatus detected successful “catch” event (the pulling force reaching the threshold value of 650 - 800 pN for *cis*-3FCP and 750-900 pN for *cis*-5FCP, while distance between probe and surface was larger than 150 nm) the controlling program was switched into the force control regime and attempted to move the AFM stage away from the probe to achieve the preset “clamp” force and to hold force constant by varying surface position for the preset time of 10 sec or until the polymer chain detaches. If the polymer chain did not detach during “force clamp”, force control was switched off, and the AFM stage was withdrawn with constant velocity. The force control feedback was

implemented by Simulink model running on DS1104 control board. Cantilever deflection and AFM stage extension were recorded at the sampling rate of 5 kHz, and the photodetector signal low-pass filter was set to 2 kHz. More details have been published by our group before.[3]

1.5 PDMS specimen preparation and mechanical testing

Procedures were adopted from previously reported literature.[4] Generally, Sylgard 184 Base (2.0 g) was added to a 20 mL scintillation vial followed by 0.2 mL of a 75 mg/mL solution of *cis*-3FCP diene (compound **1**) and diallyl 1,1'-ferrocenedicarboxylate[5] in xylenes. The solution was mixed thoroughly with a vortex mixer until completely dispersed. 0.2 g curing agent was added subsequently, and the mixture was further mixed extensively with a vortex mixer. The solution was degassed for 30 min, poured into a cylindrical Teflon mold or a PTFE surface and cured in an oven at 65 ℃ for overnight.

The obtained PDMS specimen was swollen in a phenanthroline solution (20 mg/mL in DCM) or 2,4,6-Tris(2-pyridyl)-*s*-triazine (TPTZ) solution (15 mg/mL in DCM) for overnight. Then the sample was washed with DCM to remove the phenanthroline solution on surface and dried in vacuum for overnight.

20 mm Diameter ID dry pressing die set was purchased from Across International. Split Hopkinson pressure bar test was performed on mechanophore embedded silicone specimen using method reported previously.[6]

1.6 Sonication experiments

Ultrasound experiments were conducted on Vibracell Model VCX50 sonicator at 20kHz with a 12.8 mm replaceable tip titanium probe from Sonics and Materials. Sonication was carried out on 2 mg/mL polymer solutions in THF immersed in an ice/water bath. The solutions were degassed in nitrogen for 30 min before sonication and exposed in N2 stream during the entire sonication process. Pulsed ultrasound was performed at a power of 8.7 W/cm^2 and the sonication sequence was set as 1s on 1s off.

2. Synthesis

2.1 Small molecular synthesis

2.1.1 Synthesis of *cis*-[3]ferrocenophane diene (1) and *trans*-[3]ferrocenophane diene (2)[7]

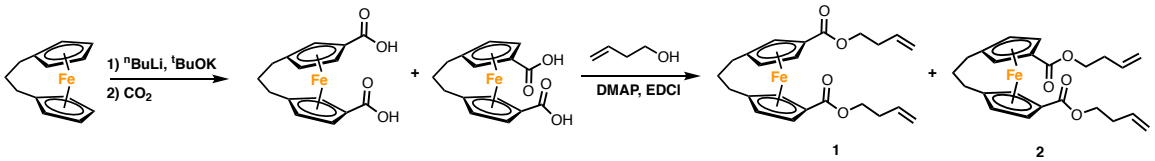

[3]ferrocenophane[1] (52 mg, 2.3 mmol) and ^{t}BuOK (0.77 g, 6.9 mmol) was dissolved in anhydrous hexane in a dry round bottle. *n*-BuLi solution (1.6M in hexane, 4.3 mL, 6.9 mmol) was put in an addition funnel and 5 mL hexane. The mixture was added dropwise to the round bottle and react for overnight under room temperature. On the second day, red precipitates were formed, and the mixture was cooled to -78 ℃. CO_2 was purged continuously to the mixture for 2h until the mixture turned from red to yellow. Then the reaction was carefully quenched with 25 mL water. The water layer was washed with benzene for 2 times while the organic layer was washed with water for 2 times. After washing, water layer was

combined and precipitated with 1M HCl solution. Yellow precipitates were collected through filtration, dried under vacuum for overnight and used directly for next step.

The mixture of acids (40.53 mg, 1.3 mmol) were dissolved in 100 mL anhydrous DCM, 3-buten-1-ol (0.68 mL, 7.8 mmol), DMAP (32 mg, 2.6 mmol) and EDCl (1.5 g, 7.8 mmol) was added subsequently. The mixture was allowed to stir for 2 days. Then 50 mL water was added to the mixture. Organic layer was washed with water for 3 times, combined and dried with anhydrous $MgSO_4$. Then the mixture was purified by flash column chromatography (ethyl acetate: hexane=1:9 as eluent). The product **1** was obtained as a red oil (25 mg, 46% yield). ^{1}H NMR (400 MHz, $CDCl_3$) δ = 5.89-5.79 (m, 2H), 5.17-5.06 (m, 4H), 4.81 (d, 2H), 4.19 (t, 4H), 4.15 (t, 2H), 2.45 (dtd, 4H), 2.04-1.89 (m, 6H). ^{13}C NMR (500 MHz, $CDCl_3$) δ = 169.56, 134.46, 117.06, 89.39, 74.75, 73.02, 71.83, 71.09, 63.29, 35.00, 33.33, 24.18. EI-MS: (m/z): 423 (M^+, 100%). The product **2** was obtained as an orange oil (4 mg, 7% yield). ^{1}H NMR (400 MHz, $CDCl_3$) δ = 5.90-5.82 (m, 2H), 5.18-5.09 (m, 4H), 4.61 (d, 2H), 4.53 (m, 2H), 4.40 (m, 2H), 4.29-4.19 (m, 4H), 2.49-2.45 (dd, 4H), 1.97 (m, 6H). ^{13}C NMR (500 MHz, $CDCl_3$) δ = 170.78, 134.37, 117.26, 89.59, 73.81, 73.58, 71.66, 63.50, 35.04, 33.40, 29.85, 24.15. EI-MS: (m/z): 423 (M^+, 100%).

2.1.2 Synthesis of *cis*-[3]ferrocenophane macrocycle (3)

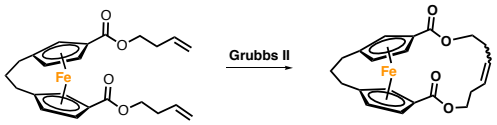

Cis-[3]ferrocenophane diene (**1**, 57.5 mg, 0.136 mmol) was dissolved in 70 mL anhydrous DCM and purged with argon for 15 min, Grubbs II catalyst (11.6 mg, 0.0136 mmol) was added as a solid and the reaction was heated to 40 °C. 1 mL of EVE were added to quench the reaction after 5 hrs. The solvent was removed, and the mixture was purified by flash column chromatography (ethyl acetate: hexane=1:3 as eluent). The product was further purified by recrystallization from ethyl acetate/hexane (v/v=1:5) and obtained as a red crystal (44 mg, 82% yield). ^{1}H NMR (400 MHz, $CDCl_3$) δ = 5.63 (td, 2H), 4.77 (d, 4H), 4.29 (ddd, 2H), 4.17-4.09 (m, 4H), 2.34 (q, 2H), 2.02-1.89 (m, 6H). ^{13}C NMR (500 MHz, $CDCl_3$) δ = 170.14, 129.30, 89.11, 76.04, 72.02, 71.55, 70.61, 63.98, 34.61, 30.89, 24.19. EI-MS: (m/z): 395 (M^+, 100%)

2.1.3 Synthesis of *trans*-[3]ferrocenophane macrocycle (4)

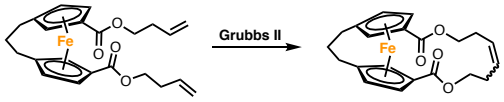

Trans-[3]ferrocenophane diene (**2**, 65 mg, 0.154 mmol) was dissolved in 80 mL anhydrous DCM and purged with argon for 15 min, Grubbs II catalyst (13.1 mg, 0.0154 mmol) was added as a solid and the reaction was heated to 40 °C. 1 mL of EVE were added to quench the reaction after 5 hrs. The solvent was removed, and the mixture was purified by flash column chromatography (ethyl acetate: hexane=1:3 as eluent). The product was further purified by recrystallization from ethyl acetate/hexane (v/v=1:5) and obtained as an orange crystal (44 mg, 82% yield). ^{1}H NMR (400 MHz, $CDCl_3$) δ = 5.57-5.55 (t, 2H), 4.65-4.64 (t, 2H), 4.51-4.50 (dd, 2H), 4.45-4.39 (m, 4H), 3.99-3.94 (td, 2H), 2.50-2.36 (m, 4H), 1.97

(m, 6H). ^{13}C NMR (500 MHz, $CDCl_3$) δ = 171.60, 128.90, 89.76, 73.52, 73.41, 72.77, 72.02, 63.82, 34.96, 31.52, 24.20. EI-MS: (m/z): 395 (M^+, 100%)

2.1.4 Synthesis of *cis*-[5]ferrocenophane diene (5)

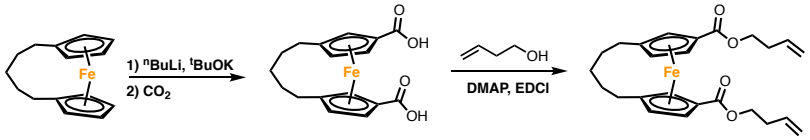

[5]ferrocenophane[2] (760 mg, 3.0 mmol) and potassium tert-butoxide (1.09 g, 9.0 mmol) were suspended in 25 mL Et_2O under argon at - 78 °C. The n-butyllithium (5.63 mL of 1.6 M solution in hexane, 9.0 mmol) was added dropwise and the solution turned into dark red. The reaction proceeded at room temperature for 3 h and then bubble the solution with CO_2 overnight at - 78 °C. Dissolve the crude suspension with 100 mL water and wash with 100 mL hexane for 3 times. Precipitate the diacid out by adding 50 mL 2M HCl solution dropwise and wash the yellow solid with DI water. Mixture of acids were collected as a yellow solid (765 mg, 75% yield).

The diacid mixture (300 mg, 0.88 mmol), 3-buten-1-ol (0.39 mL, 4.39 mmol), EDCl (1.0 g, 5.28 mmol) and DMAP (197 mg, 1.76 mmol) were dissolved in 20 mL DCM, the flask of which was flame-dried and filled with nitrogen. The reaction proceeded at room temperature for 2 days. After reaction, the solvent was evaporated out and the crude product was separated by silica gel column chromatography (polarity of mobile phase increased gradually from pure hexane to EtOAc : hexane = 1: 19). Prouct was collected as a red oil (220 mg, 56% yield). ^{1}H NMR (400 MHz, $CDCl_3$) δ=5.91-5.80 (m, 2H), 5.17-5.07 (m, 4H), 4.81 (s, 2H), 4.71 (s, 2H), 4.26-4.22 (m, 4H), 4.16 (s, 2H), 2.48-2.43 (m, 4H), 2.53-2.29 (m, 4H), 2.23-2.16 (M, 2H), 1.85-1.82 (m, 4H) ; ^{13}C NMR (400 MHz, $CDCl_3$) δ=169.70, 134.43, 116.86, 92.57, 73.45, 71.36, 70.97, 69.55, 63.16, 33.18, 24.57, 24.56, 24.32. EI-MS: (m/z): 451 (M^+, 100%).

2.1.5 Synthesis of *cis*-[5]ferrocenophane macrocycle (6)

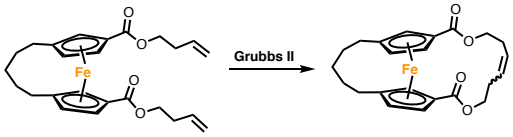

Cis-[5]ferrocenophane diene (**5**, 160 mg, 0.355 mmol) and Grubbs II catalyst (18.4 mg, 0.02 mmol) were dissolved in 200 mL anhydrous DCM in a nitrogen-filled, dry flask. The reaction proceeded at 40 °C overnight and several drops of ethyl vinyl ether were added to quench the reaction. Then the solvent was evaporated and the crude product was separated by silica gel column chromatography (polarity of mobile phase increased gradually from pure hexane to EtOAc : hexane = 1: 4). Subsequent recrystallization with EtOAc and hexane gave a red crystal (105 mg,70 % yield)**.** ^{1}H NMR (400 MHz, $CDCl_3$) δ=5.75-5.72 (m, 2H), 4.81(dd, J = 1.6, 1.2 Hz, 2H), 4.69 (t, J = 1.2 Hz, 2h), 4.33-4.21 (m, 4H), 4.19 (dd, J = 1.6 Hz, 1.2 Hz, 2H), 2.36-2.33 (m, 8H), 2.33 (s, 2H), 1.90-1.71 (m, 4H) ; ^{13}C NMR (400 MHz, $CDCl_3$) δ=170.43, 129.16, 92.29, 74.33, 71.29, 71.06, 69.82, 63.84, 30.66, 25.02, 24.59, 24.43. EI-MS: (m/z): 423 (M^+, 100%).

2.2 Polymer synthesis

2.2.1 Synthesis of *cis*-[3]ferrocenophane-*co*-epoxy COD (7)

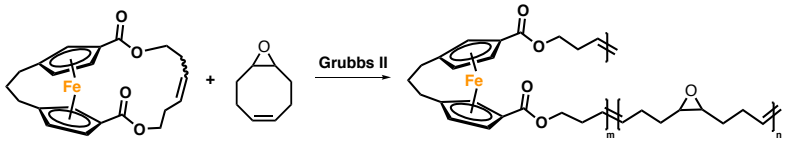

Cis-[3]ferrocenophane macrocycle (**3**, 12mg, 0.03 mmol) and epoxy-COD (42 mg, 0.13 mmol) was dissolved in 0.2 mL anhydrous DCM. The solution was purged with argon for 15 min. 0.01 mL of Grubbs II solution in DCM (0.4 mL, 20 mg/mL) was added to initiate the polymerization. After the reaction mixture was stirred at room temperature overnight, several drops of EVE were added to stop polymerization. The polymer solution was precipitated into methanol 3 times. The polymer was collected by filtration, dried under high vacuum for overnight. Product **7** was obtained as a yellow solid (43 mg, 80%).

2.2.2 Synthesis of *trans*-[3]ferrocenophane-*co*-epoxy COD (8)

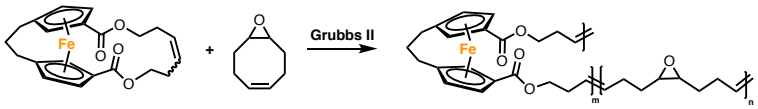

Trans-[3]ferrocenophane macrocycle (**4**, 6 mg, 0.015 mmol) and epoxy-COD (45 mg, 0.14 mmol) was dissolved in 0.2 mL anhydrous DCM. The solution was purged with argon for 15 min. 0.01 mL of Grubbs II solution in DCM (0.4 mL, 21 mg/mL) was added to initiate the polymerization. After the reaction mixture was stirred at room temperature overnight, several drops of EVE were added to stop polymerization. The polymer solution was precipitated into methanol 3 times. The polymer was collected by filtration, dried under high vacuum for overnight. Product **8** was obtained as a yellow solid (36 mg, 70% yield).

2.2.3 Synthesis of *cis*-[5]ferrocenophane-*co*-epoxy COD (9)

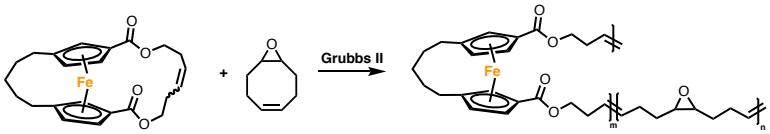

Cis-[5]ferrocenophane macrocycle (**6**, 20 mg, 0.047 mmol) and epoxy-COD (21 mg, 0.06 mmol) was dissolved in 0.15 mL anhydrous DCM. The solution was purged with argon for 15 min. 0.01 mL of Grubbs II solution in DCM (0.4 mL, 13 mg/mL) was added to initiate the polymerization. After the reaction mixture was stirred at room temperature overnight, several drops of EVE were added to stop polymerization. The polymer solution was precipitated into methanol 3 times. The polymer was collected by filtration, dried under high vacuum for overnight. Product **9** was obtained as a yellow solid (31 mg, 75% yield).

2.2.4 Synthesis of *cis*-[3]ferrocenophane-*co*-ferrocene-*co*-epoxy COD (10)

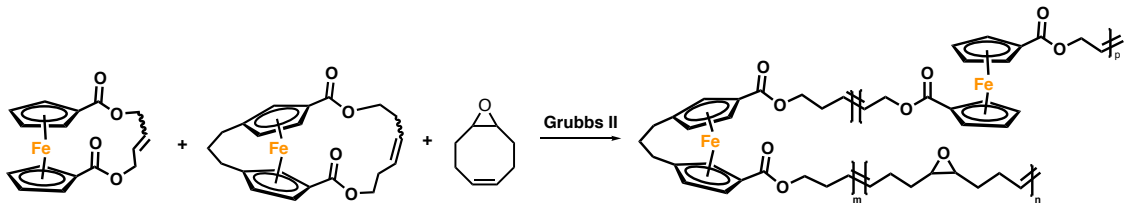

Cis-[3]ferrocenophane macrocycle (**6**, 16 mg, 0.04 mmol), ferrocene macrocycle (13.2 mg, 0.04 mmol) and epoxy-COD (25.2 mg, 0.2 mmol) was dissolved in 0.2 mL anhydrous DCM. The solution was purged with argon for 15 min. 0.02 mL of Grubbs II solution in DCM (0.4 mL, 6 mg/mL) was added to initiate the polymerization. After the reaction mixture was stirred at room temperature overnight, several drops of EVE were added to stop polymerization. The polymer solution was precipitated into methanol 3 times. The polymer was collected by filtration, dried under high vacuum for overnight. Product **10** was obtained as a yellow solid (46 mg, 84% yield).

2.2.5 Synthesis of *cis*-[3]ferrocenophane-*co*-*g*DCC (11)

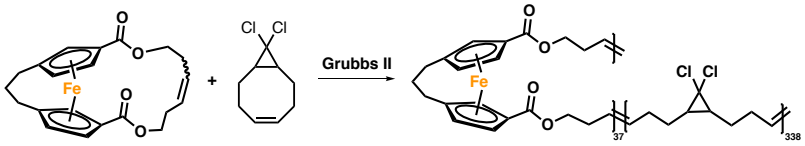

Cis-[3]ferrocenophane macrocycle (**3**, 12mg, 0.03 mmol) and gDCC-cyclooctene (42 mg, 0.22 mmol) was dissolved in 0.2 mL anhydrous DCM. The solution was purged with argon for 15 min. 0.01 mL of Grubbs II solution in DCM (0.4 mL, 20 mg/mL) was added to initiate the polymerization. After the reaction mixture was stirred at room temperature for 3 h, several drops of EVE were added to stop polymerization. The polymer solution was precipitated into methanol 3 times. The polymer was collected by filtration, dried under high vacuum for overnight. Product **11** was obtained as a yellow solid (43 mg, 80%).

3. Modeling of polymer extension (CoGEF)

CoGEF analysis was conducted following previous procedure using software SPARTAN' 10.[8] The end-end distance between two ends of the monomer (before and after activation) was constrained and the monomer structure deformed by increasing the end-end distance to the extent where the relative energy of the molecule is approximately 500 kJ/mol higher than that of equilibrium geometry. Then the constrained distance was released iteratively (~ 0.01 nm per step), and the relative energy of each step was determined. The analysis was conducted three times and average value was obtained for the contour length change.

Detailed modeling procedure can be found in previously reported methods.[8]

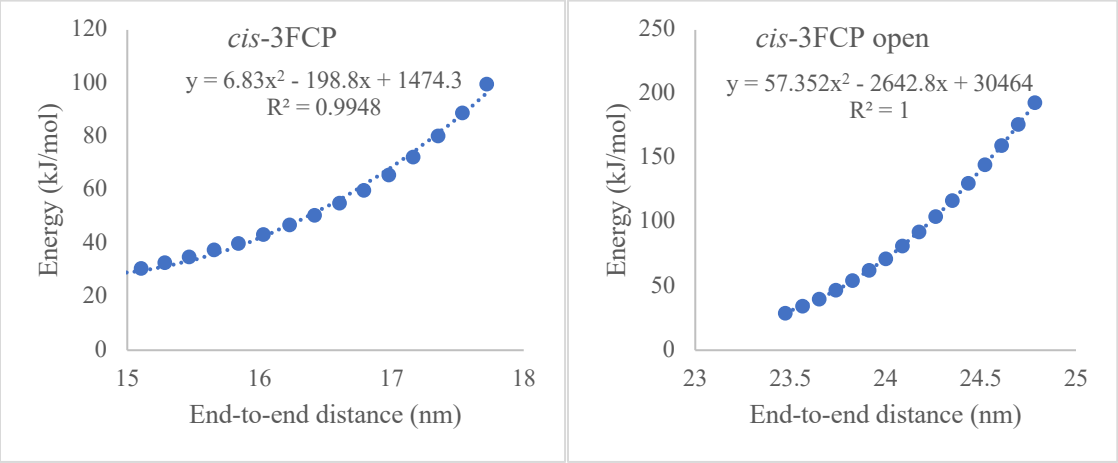

Figure S1. Example CoGEF analysis of *cis*-3FCP. The energies at each step are plotted vs. constraint distance (displacement) and fit with a quadratic (blue) to obtain the function of energy vs. displacement. The derivative of the fit provides a linear function of force vs. distance, which upon extrapolation to zero force provides the effective force-free end-to-end distance.

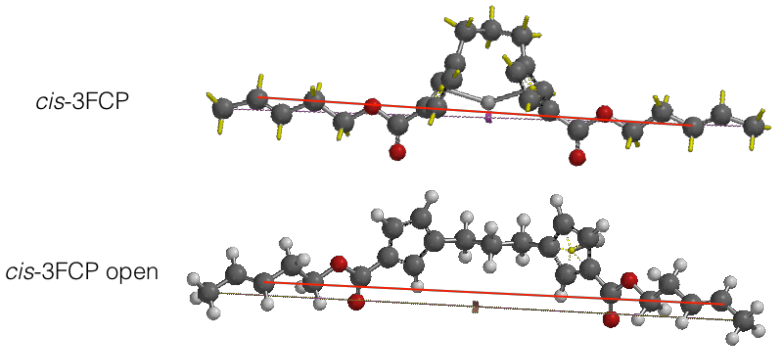

Figure S2. *Cis*-3FCP monomer structures with end-to-end distance indicated (red line).

Table S1. Force-free end-to-end distance of *cis*-[3]ferrocenophane

Entry	Try 1 (nm)	Try 2 (nm)	Try 3 (nm)	Average (nm)
L_1	1.46	1.44	1.45	1.45
L_2	2.30	2.31	2.31	2.31
L_2-L_1	-	-	-	0.86

Table S2. Force-free end-to-end distance of *trans*-[3]ferrocenophane

Entry	Try 1 (nm)	Try 2 (nm)	Try 3 (nm)	Average (nm)
L_1	1.64	1.64	1.65	1.64
L_2	2.25	2.25	2.30	2.27
L_2-L_1	-	-	-	0.63

Table S3. Force-free end-to-end distance of cis-[5]ferrocenophane

Entry	Try 1 (nm)	Try 2 (nm)	Try 3 (nm)	Average (nm)
L_1	1.72	1.79	1.85	1.79

L_2	2.74	2.75	2.73	2.74
L_2-L_1	-	-	-	0.95

Table S4. Force-free end-to-end distance of epoxy-COD

Entry	All-*cis* (nm)	All-*trans* (nm)	Average (nm)
1	0.90	0.92	0.91

The ratio of polymer contour lengths, $L_{final}/L_{initial}$ are obtained from the following equation,

$$\frac{L_{final}}{L_{initial}} = \frac{(L_2 \times x) + (L_{epoxy-COD} \times (1-x))}{(L_1 \times x) + (L_{epoxy-COD} \times (1-x))}$$

where x denotes the molar fraction of FCP within the polymer as determined by 1H-NMR spectroscopy, and L refers the end-to-end distance obtained from CoGEF calculations for the various monomers. A summary of simulation results is shown in Table S5.

Table S5. Ratio of Polymer lengths before and after plateau

Entry	FCP molar ratio, x[a]	$L_{final}/L_{initial}$	
		SMFS[b]	modeling
***cis*-3FCP**	0.12	1.08 ± 0.06	1.10
	0.16	1.15 ± 0.02	1.14
***trans*-3FCP**	0.06	1.06 ± 0.02	1.04
***cis*-5FCP**	0.15	1.13 ± 0.09	1.13
	0.35	1.30 ± 0.05	1.27

[a]Molar ratio of **FCP**s in copolymer is determined from ^{1}H NMR integration. [b]Values are averages of the ratio of contour length after and before transition determined by fitting force curves to the freely jointed chain model.

Numbers of ferrocene units per chain are obtained from the following equation,

$$\#\text{ of ferrocene units} = \frac{L_{initial} \times x_{FC}}{L_{cis-3FCP} \times x_{cis-3FCP} + L_{FC} \times x_{FC} + L_{epoxy-COD} \times x_{epoxy-COD}}$$

where x denotes the molar fraction of various monomers within the polymer as determined by 1H-NMR spectroscopy, and L refers the force-free end-to-end distance obtained from CoGEF calculations for the various monomers. $L_{initial}$ refers to the initial polymer contour length before transition. A summary of simulation results is shown in Table S9.

4. SMFS data list

4.1 SMFS Data list for *cis*-[3]ferrocenophane-*co*-epoxy COD

Table S6. Parameters obtained for *cis*-[3]ferrocenophane

Entry	x[a]	*f**	$x^{\ddagger}$ (nm) BE	$x^{\ddagger}$ (nm) cusp	L_1(nm)	L_2(nm)	L_2/L_1	Kuhn Length	$E_{initial}$	E_{final}
1	0.17	817.5	0.073	0.249	427.8	513.4	1.20	0.34	2.5E+04	7.6E+04
2	0.17	784.3	0.076	0.260	359.7	434.3	1.21	0.41	1.7E+04	5.5E+04
3	0.17	838.2	0.074	0.249	300.8	374.6	1.24	0.33	2.1E+04	5.7E+04
4	0.17	821.5	0.073	0.251	379.7	444.2	1.17	0.43	1.7E+04	3.0E+04

5	0.17	799.6	0.074	0.252	515.2	584.3	1.13	0.30	2.8E+04	5.4E+04
6	0.17	841.4	0.073	0.243	186.4	224.2	1.20	0.30	3.0E+04	1.2E+05
7	0.17	766.9	0.075	0.256	423.7	510.5	1.20	0.36	2.1E+04	5.2E+04
8	0.17	819.0	0.078	0.254	205.8	235.9	1.15	0.32	2.8E+04	5.1E+04
9	0.17	781.2	0.074	0.254	335.3	428.8	1.28	0.52	9.5E+03	3.8E+04
10	0.17	783.7	0.080	0.264	182	205.1	1.13	0.24	5.8E+04	1.3E+05
11	0.13	779.5	0.081	0.272	260.9	282.6	1.08	0.17	7.9E+04	7.5E+04
12	0.13	827.3	0.081	0.266	105	107	1.02	0.16	2.2E+05	6.7E+04
13	0.13	826.6	0.073	0.250	414.5	468.4	1.13	0.35	2.9E+04	5.3E+04

4.2 SMFS Data list for *trans*-[3]ferrocenophane-*co*-epoxy COD

Table S7. Parameters obtained for *trans*-[3]ferrocenophane

Entry	x[a]	*f**	x‡ (nm) BE	x‡ (nm) cusp	L_1(nm)	L_2(nm)	L_2/L_1	Kuhn Length	$E_{initial}$	E_{final}
1	0.07	1156.4	0.059	0.184	324.1	350.2	1.08	0.46	2.7E+04	5.0E+04
2	0.07	1154.5	0.060	0.181	344.1	368.5	1.07	0.44	3.2E+04	7.2E+04
3	0.07	1113.5	0.063	0.191	178.7	185.9	1.04	0.43	2.5E+04	2.9E+04
4	0.07	1154.8	0.061	0.185	400.7	419.4	1.05	0.40	4.9E+04	4.9E+04
5	0.07	1123.1	0.061	0.183	185.8	201.6	1.08	0.40	6.4E+04	6.4E+04
6	0.07	1201.2	0.062	0.184	264.2	274.6	1.04	0.35	5.9E+04	5.9E+05
7	0.07	1122.0	0.059	0.180	219.6	236.8	1.08	0.41	6.4E+04	6.4E+04
8	0.07	1117.3	0.062	0.186	317.2	337.1	1.07	0.42	5.5E+04	5.5E+04

4.3 SMFS Data list for cis-[5]ferrocenophane-*co*-epoxy COD

Table S8. Parameters obtained for *cis*-[5]ferrocenophane

Entry	x[a]	*f**	x‡ (nm) BE	x‡ (nm) cusp	L_1 (nm)	L_2 (nm)	L_2/L_1	Kuhn Length	$E_{initial}$	E_{final}
1	0.15	965.7	0.075	0.241	308.4	330.0	1.08	0.16	9.9E+04	1.3E+05
2	0.15	944.8	0.084	0.242	324.5	389.2	1.19	0.17	4.3E+04	8.9E+04
3	0.30	1020.0	0.079	0.225	274.4	330.0	1.20	0.19	1.0E+05	1.8E+05
4	0.30	968.4	0.085	0.229	284.6	347.7	1.22	0.19	8.5E+04	1.7E+05
5	0.30	925.3	0.081	0.234	406.2	505.9	1.24	0.29	3.8E+04	9.2E+04
6	0.40	968.5	0.105	0.233	127.0	160.1	1.26	0.19	1.0E+05	2.7E+05
7	0.40	915.2	0.111	0.240	269.8	360.6	1.34	0.26	4.6E+04	1.2E+05

4.4 SMFS data list for *cis*-[3]ferrocenophane-*co*-ferrocene-*co*-epoxy COD

Table S9. Parameters obtained for *cis*-[3]ferrocenophane-*co*-ferrocene-*co*-epoxy COD

Entry	L_1(nm)	L_2(nm)	DP	# of ferrocene units	Kuhn Length	$E_{initial}$	E_{final}

1	201.3	210.5	174.5	21.7	0.41	2.2E+04	2.0E+04
2	194.4	206.0	170.7	21.0	0.40	1.9E+04	2.1E+04
3	257.6	289.6	240.0	27.8	0.46	1.6E+04	3.4E+04
4	251.0	280.0	232.0	27.1	0.37	2.0E+04	4.2E+04
5	522.3	579.9	480.6	56.3	0.35	2.6E+04	5.1E+04
6	364.1	391.1	324.2	39.3	0.32	2.9E+04	3.3E+04
7	124.4	137.0	113.6	13.4	0.34	2.3E+04	4.6E+04
8	275.3	307.4	254.8	29.7	0.50	1.5E+04	3.3E+04
9	329.3	361.3	299.5	35.5	0.43	1.7E+04	3.0E+04
10	102.0	102.5	85.0	11.0	0.23	6.0E+04	3.4E+04
11	358.4	365.4	302.9	38.7	0.28	3.2E+04	2.2E+04
12	196.6	213.3	176.8	21.2	0.41	1.7E+04	2.5E+04
13	302.8	326.6	270.7	32.7	0.24	5.1E+04	8.0E+04
14	197.6	228.4	189.3	21.3	0.40	1.5E+04	4.5E+04
15	524.4	554.4	459.5	56.6	0.38	2.0E+04	2.2E+04
16	188.7	206.8	171.3	20.4	0.28	3.7E+04	6.5E+04
17	304.2	343.5	284.7	32.8	0.40	2.0E+04	4.9E+04
18	173.3	180.5	149.6	18.7	0.18	6.9E+04	7.5E+04
19	393.3	462.2	383.1	42.4	0.36	1.6E+04	5.6E+04
20	132.0	142.3	117.9	14.2	0.30	3.4E+04	5.4E+04
21	109.2	118.2	98.0	11.8	0.29	3.8E+04	7.4E+04
22	419.1	450.4	373.3	45.2	0.29	3.3E+04	6.1E+04

5. Rate-force relationships

5.1 Rate-force relationship of ferrocene[9]

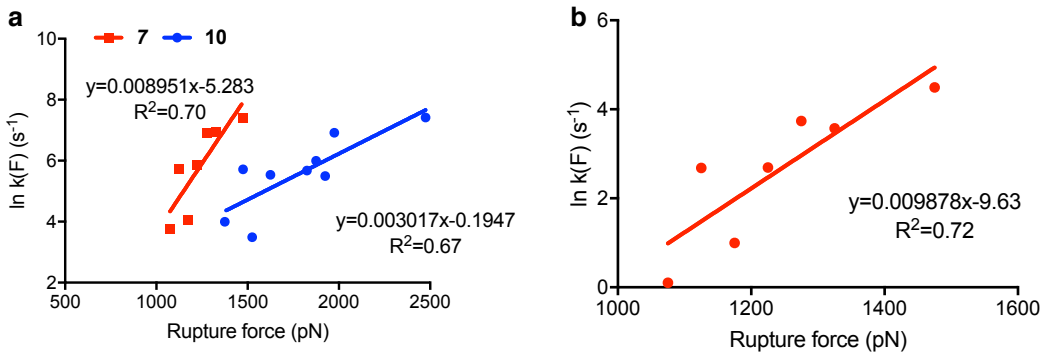

Figure S3. (a) Rate-force data for chain scission/detachment of **7** (red) and **10** (blue) with linear regressions. (b) Rate-force data for ferrocene dissociation taking the statistical presence of multiple ferrocenes along the trapped polymer chain into account.

5.2 Rate-force relationships of *trans*-[3]ferrocenophane

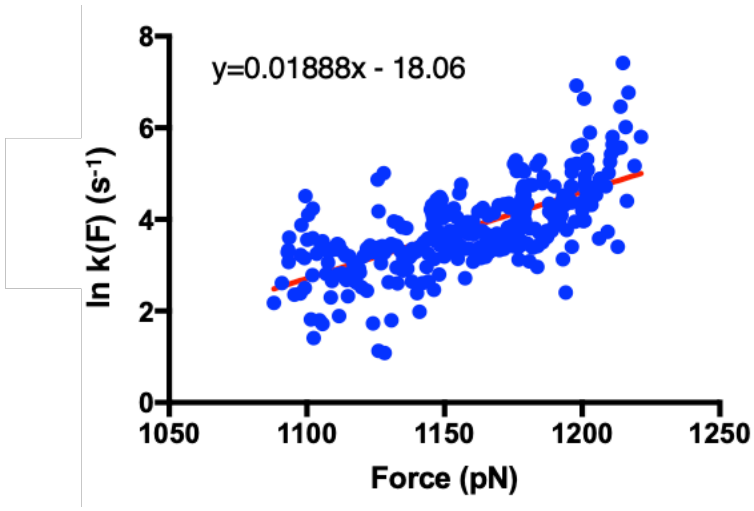

Figure S4. Force-rate data from all *trans*-3FCP curves with a linear regression (red straight line).

6. Force-clamping experiments data processing

Extension data obtained in the force clamp regime were fitted with a single exponent in Matlab using Levenberg-Marquardt nonlinear least squares algorithm.

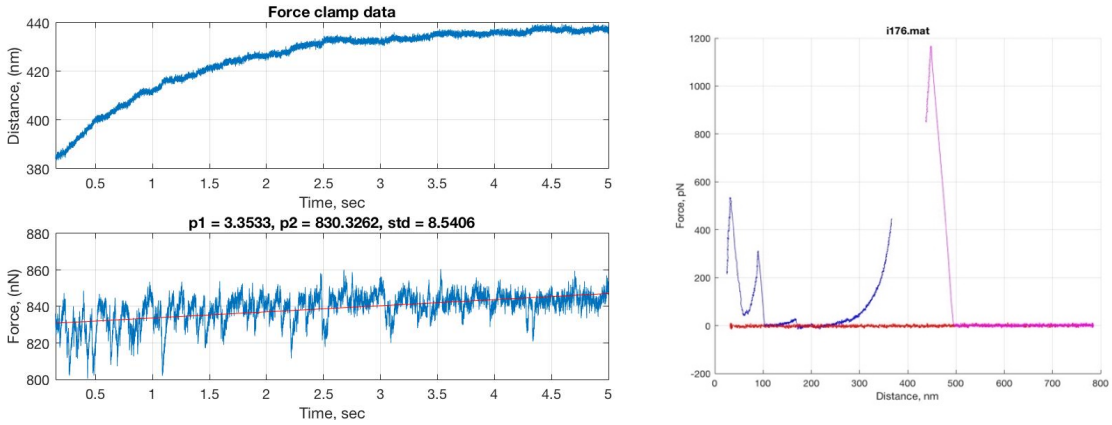

Figure S5. Representative data of force clamp experiments. The figure on the left shows data collected during time interval when force was held at a constant value. The figure on the right shows corresponding constant velocity data before and after force control engagement.

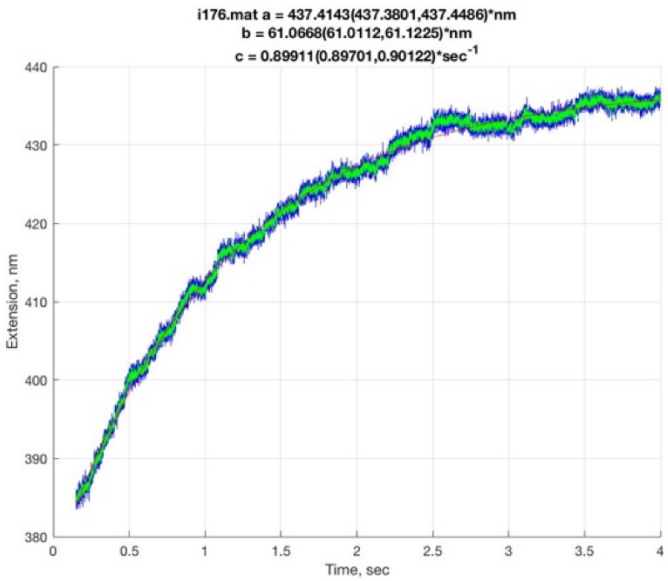

Figure S6. Representative data of a single exponent fit during the constant-force regime is defined by equation $\boldsymbol{y = a + b * e^{-c*x}}$

Table S10. Results of fitting force clamp extension data of *cis*-3FCP with single exponent $y = a + b * e^{-c*x}$

Entry	Force (pN)	c (s-1)	ln(c)
1	683	0.994	-0.006
2	711	1.181	0.166
3	726	1.724	0.545
4	691	1.130	0.122
5	704	1.067	0.0651
6	762	1.985	0.685
7	660	0.155	-1.865
8	678	0.432	-0.839
9	785	2.593	0.953
10	719	1.393	0.332
11	733	1.510	0.412
12	771	2.126	0.754
13	765	2.232	0.803
14	758	2.472	0.905
15	707	0.682	-0.382
16	710	0.742	-0.298

Table S11. Results of fitting force clamp extension data of *cis*-5FCP with single exponent $\boldsymbol{y = a + b * e^{-c*x}}$

Entry	Force (pN)	c (s-1)	ln(c)
1	871	1.210	0.191
2	869	1.420	0.351
3	830	0.899	-0.106
4	811	0.488	-0.716
5	818	0.598	-0.514
6	815	0.526	-0.642

7	819	0.599	-0.513
8	772	0.321	-1.135
9	770	0.194	-1.639
10	796	0.479	-0.736
11	838	0.500	-0.694
12	851	1.255	0.227
13	863	2.082	0.733
14	856	0.510	-0.673
15	832	1.450	0.372

7. Ring strain calculation

Table S12. Force free activation energy calculated for ferrocene and ferrocenophanes

Entry	Tilt angle	Ring strain (kcal/mol)[a]	$\Delta G_0^{\ddagger}$ (model, kcal/mol)	$\Delta G_0^{\ddagger}$ (thermal, kcal/mol)
FC	0	0	-	54.8[10]
2FCP	21.6[11]	12.1	42.7	<46[c]
3FCP	7.6[12]	2.8	52.0	-
5FCP	1.7[b]	0.7	54.1	-

[a] Calculated by adapting the total energy-tilt angle relationship from literature.[13]

[b] Structure used was optimized by DFT.

[c] Estimated from reported thermodynamic data from literature.[14,15]

8. Determination of force-free rate constant of *cis*-3FCP

Upon heating at high temperature, *cis*-3FCP will isomerize to *trans*-3FCP and decompose as a result of Fe-Cp bond breakage. The activation energy of this reaction gives a lower limit of *cis*-3FCP force-free activation energy.

$$\textit{cis}\text{-3FCP} \xrightarrow{k_1} \text{decomposition}$$

A mix of *cis*-3FCP methyl ester and *trans*-3FCP methyl ester (20 mg) was dissolved in 1 mL *cis*-decalin in a pressured vessel and heated to 220 °C. At each time point, the solution was allowed to cool down to room temperature. 0.1 mL aliquots were taken out and dissolved in 0.5 mL $CDCl_3$ followed by the addition of 30 μL benzoic acid solution (100 mg/mL in $CDCl_3$) as internal standard. ^{1}H NMR spectra were taken for each time point and the total amount of *cis*-3FCP *and trans*-3FCP was monitored as shown by Figure S1. Results are summarized in Table S2.

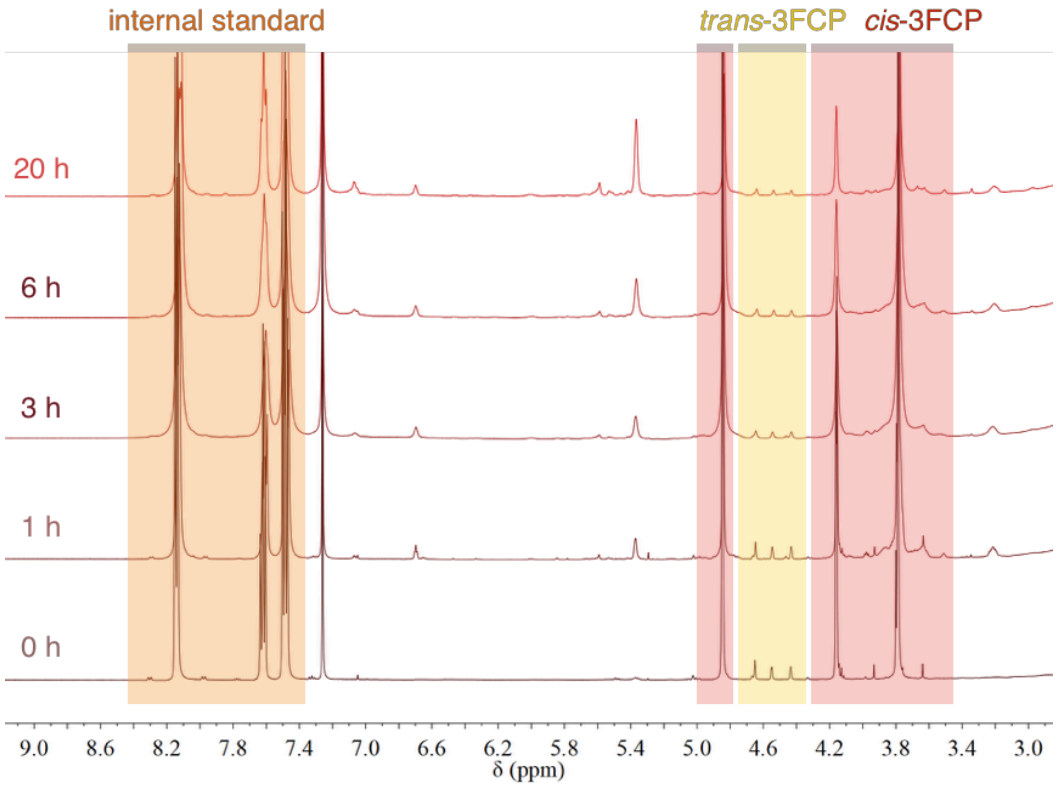

Figure S7. Overlay of ^{1}H NMR spectra of *cis*-, *trans*-3FCP methyl ester mixtures under heating at 220 °C for different times (normalized by the peak area of internal standard; δ=7.9-8.4 ppm).

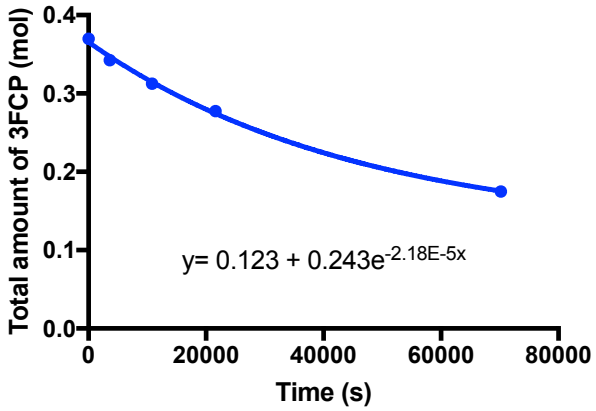

Figure S8. Total amount of *cis*-3FCP and *trans*-3FCP relative to internal standard change with time; fitted with one phase exponential decay.

Table S13. Summary of force-free rate constant and activation energy of *cis*-3FCP

Entry	k_1 (s^{-1})	$\Delta G_0^{\ddagger}$ (kcal/mol)	k_0 (at RT, s^{-1})
cis-3FCP	2.18E-5	39.9	2.95E-17
cis-5FCP	-	42.0[a]	1.01E-18

[a]Derived from the $\Delta G_0^{\ddagger}$ of *cis*-3FCP and the reported difference of ring strain between *cis*-3FCP and *cis*-5FCP according to Table S12.

9. Summary of SMFS parameters

Table S14. SMFS Parameters Obtained by Modeling Force-Extension Curves with Bell-Evans Model

Entry	Force clamping		$\Delta G^{\ddagger}$ (kcal/mol)[a]	Constant velocity	
	$\Delta x^{\ddagger}$ (Å)	k_0 (s^{-1})		$\Delta x^{\ddagger}$ (BE) (Å)	k_0 (s^{-1})
cis-3FCP	0.77	5.29E-6	24.8	0.76±0.03	9.41E-6
trans-3FCP	-	1.20E-6	25.7	0.69±0.01	2.09E-7
cis-5FCP	0.81	6.69E-8	27.4	0.88±0.14	9.50E-8

[a] Force-free activation energy were obtained by extrapolating rate-force data collected from force clamping experiments to F=0 N

10. CoGEF modeling of force-free activation length of transition states

Transition states were taken as the geometry just before breaking (*cis*-3FCP: stretched distance = 14 Å; *trans*-3FCP: stretched distance = 11.5 Å; *cis*-5FCP: stretched distance = 14 Å). All carbon atoms on the Cp ring of the ground states were frozen and four carbon atoms on the Cp ring (C_2, C_3, C_4, C_5) of the transition states were frozen during CoGEF analysis to account for the distortion of Cp ring during stretching.

Table S15. Summary of force-free activation length obtained by CoGEF modeling and force-free rate constants obtained by fitting with a cusp model

Entry	L_{GS} (nm)	L_{TS} (nm)	$\Delta x^{\ddagger}$ (nm)	$\Delta G^{\ddagger}$ (cusp, kcal/mol)	k_0 (cusp, s^{-1})
cis-3FCP	13.90±0.11	16.92±0.04	3.02±0.12	42-43	1.87E-19-1.01E-18
trans-3FCP	14.87±0.17	17.03±0.02	2.16±0.17	41-42	1.01E-18-5.46E-18
cis-5FCP	14.24±0.02	17.10±0.15	2.85±0.15	45-46	1.18E-21-6.38E-21

11. Silicone elastomer embedded with *cis*-3FCP and ferrocene

11.1 Drop test

A *cis*-3FCP/ferrocene embedded silicone plus is placed inside a 20 mm diameter hardened steel dry compression die. An iron bar weighted at 6.38 kg was held 10 cm above the compression die. Then the weight is released and dropped freely. Let it hit the compression die.

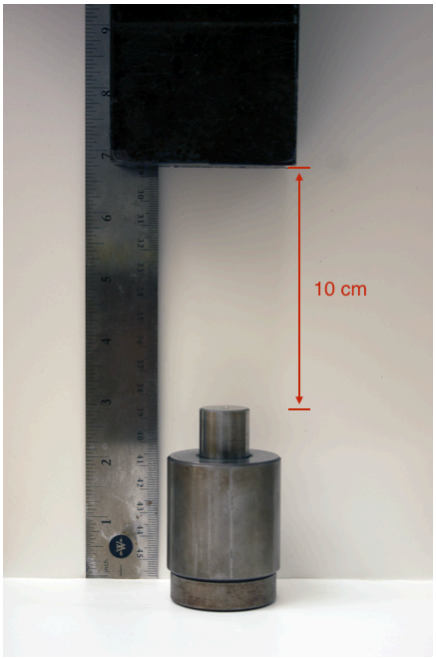

Figure S9. Drop test illustration. The distance between the compression die and the weight is 10 cm.

11.2 Split Hopkinson pressure bar test

A polycarbonate split Hopkinson bar is used to generate repeatable, measured impact loading on both the *cis*-3FCP and FC specimens. The measured average peak stress and strain values are show in Table S16 to verify that all specimens were subjected to similar loading.

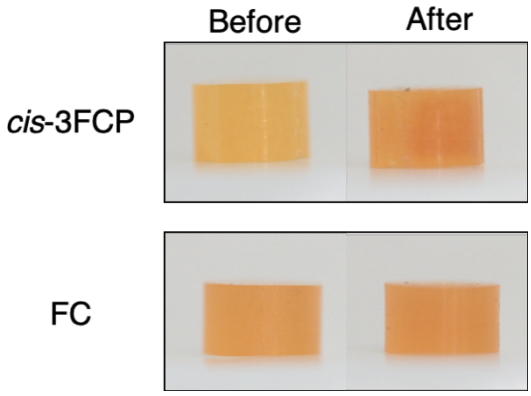

Figure S10. Representative photos of *cis*-3FCP (top) and FC (bottom) embedded silicone specimen that were before (left) and after (right) a split Hopkinson pressure bar test with similar experimental parameters.

Table S16. Average peak stress and strain of *cis*-3FCP and FC embedded silicone specimen for the split Hopkinson pressure bar test

Entry	Peak stress (MPa)	Peak strain
cis-3FCP	19.46±3.08	0.60±0.10
FC	18.44±1.98	0.57±0.07

11.3 Activation by uniaxial tension

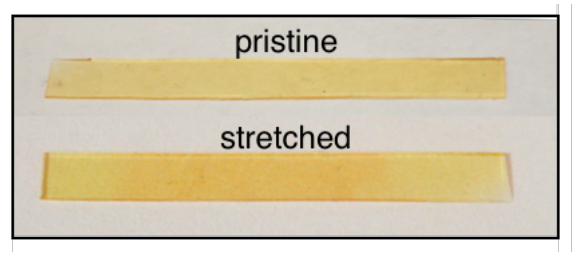

Figure S11. Uniaxial stretching (~100% strain) of a *cis*-3FCP containing PDMS film.

11.4 UV-vis spectrum of silicon elastomer after stretching

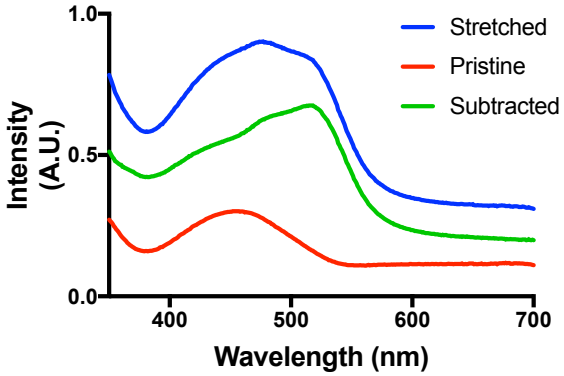

Figure S12. Normalized UV-vis spectrum of silicone elastomer embedded with *cis*-3FCP before and after stretching

11.5 Demonstration of versatile color change

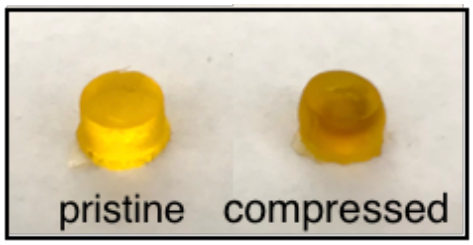

Figure S13. Pristine (left) and compressed (right) *cis*-3FCP embedded silicone plug that contains TPTZ as an exogenous ligand.

12. Demonstration of crosslinking

12.1 Sonication of 9

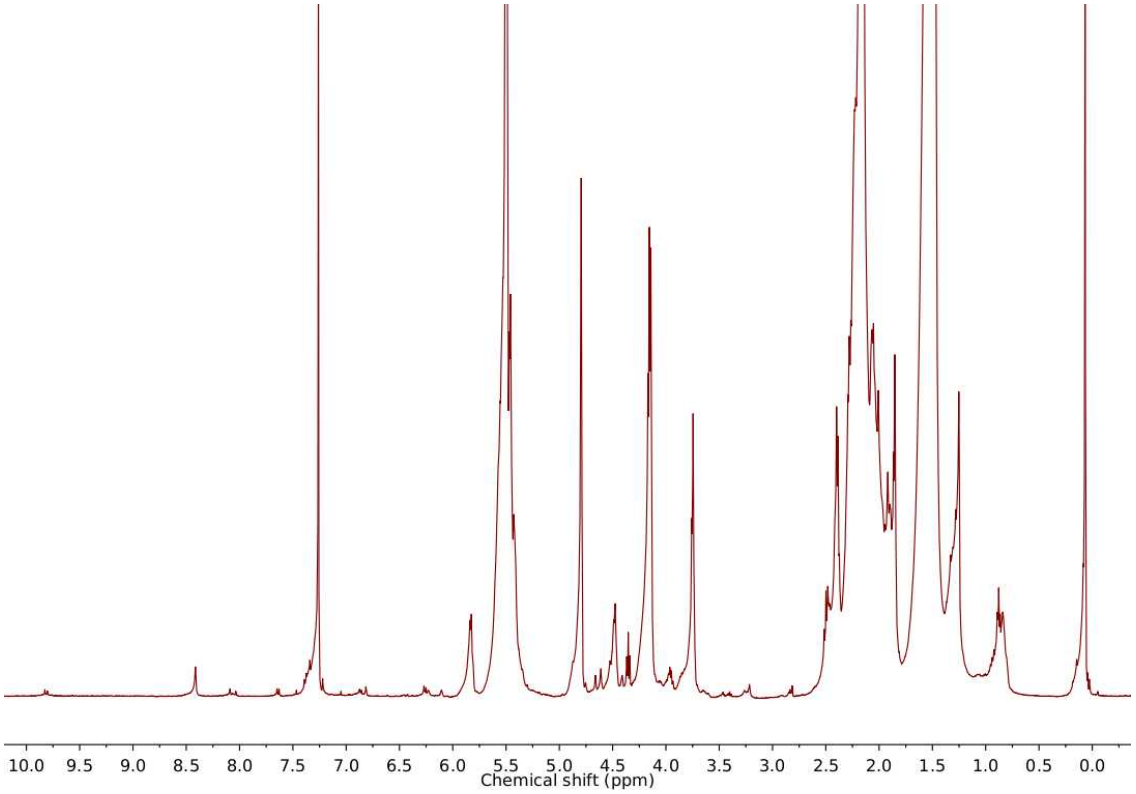

Figure S14. ^{1}H NMR spectrum for the soluble part of 9 after 30 min. Peak for Cp (δ=6.6, 6.7, 7.4 ppm) is not observed.

12.2 Sonication of 11 with pyrenyl-maleimide

26 mg **11** and 125 mg pyrenyl-maleimide (3 equivalence of total amount of *cis*-[3]ferrocenophane) were dissolved and sonicated in 13 mL THF. Aliquot was taken out after 2 h. Solvent was removed and washed with MeOH for 2 times. The polymer was redissolved in THF and injected directly into GPC. The proposed DA reaction process is shown in Scheme S1.

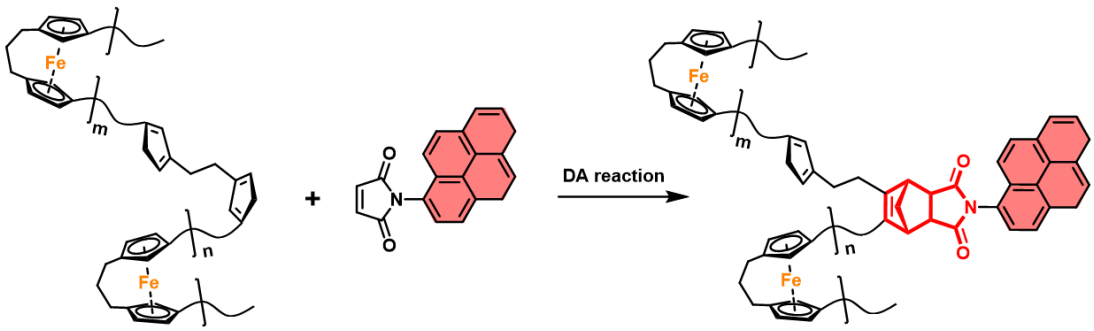

Scheme S1. DA mechanism of Cp with pyrenyl-maleimide.

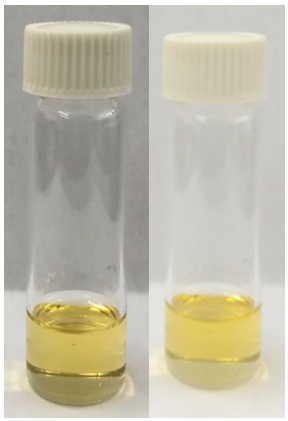

Figure S15. Photos of polymer solution with pyrenyl-maleimide before (left) and after 30 min sonication (right).

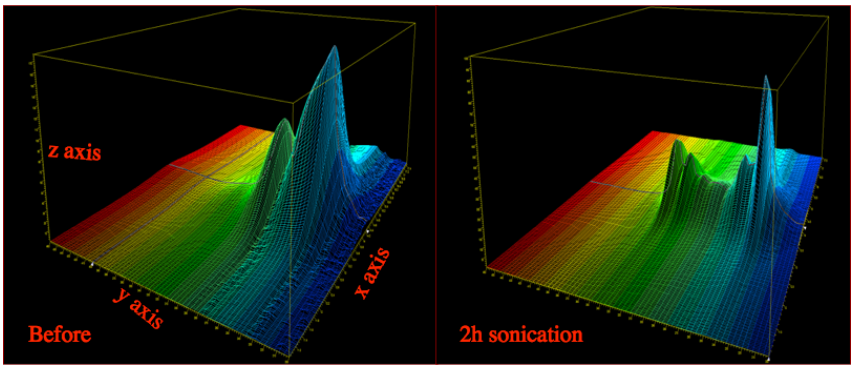

Figure S16. UV signals of **11** before and after 2h sonication in the presence of pyrenyl-maleimide. X axis represents retention time (11-17 min), Y axis represents wavelength (200-460 nm), Z axis represents intensity.

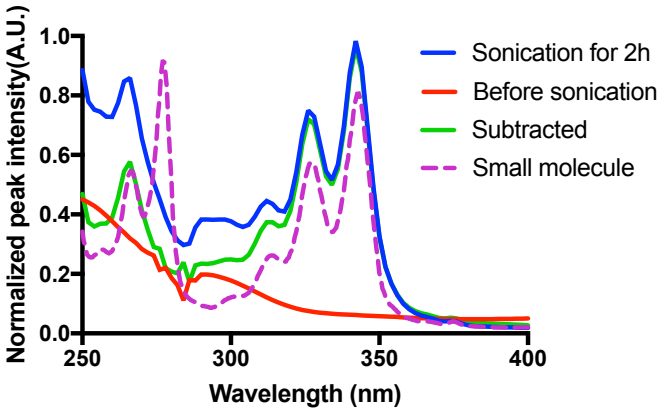

Figure S17. Absorbance spectrum of **11** in the presence of pyrenyl-maleimide (10 mg/mL) at retention time = 14.4 min.

13. DFT calculation

13.1 Computational methods

The stretched structure evolution of ferrocene was explored with Gaussian 09. 1,1'-ferrocenedicarboxylic allyl diester was selected as the model compound for calculation because it well matches with the structure unit in the polymer chain for this study. Very recently, Li et al. used DFT calculation to simulate the elongation process from external force on ferrocene, and the simulation results agreed with experiment results.6 Based on this benchmark calculation study, we utilized the same DFT calculation method: UB97D function was employed to describe the system, along with the def2-svp basis sets for C, H, and O atoms and the more extensive def2-tzvp basis set for Fe. Solvent effects (THF) were included using the SMD implicit solvation model. CoGEF (constrained geometry simulates external force) method proposed by Beyer et al was used to model the contour length.7 Briefly, the end-to-end distance of the model compound was fixed to specific values to mimic the imposed force, meanwhile all other geometric coordinates were allowed to fully relax. Then equilibrium geometry and energy were determined at iteratively increased end-to-end distance until the good separation between molecular segments after chain scission. The relationship of force and elongated distance can be obtained from a curve of the 1st derivate of energy to distance. The fully relax model compound energy was normalized to 0 kJ/mol.

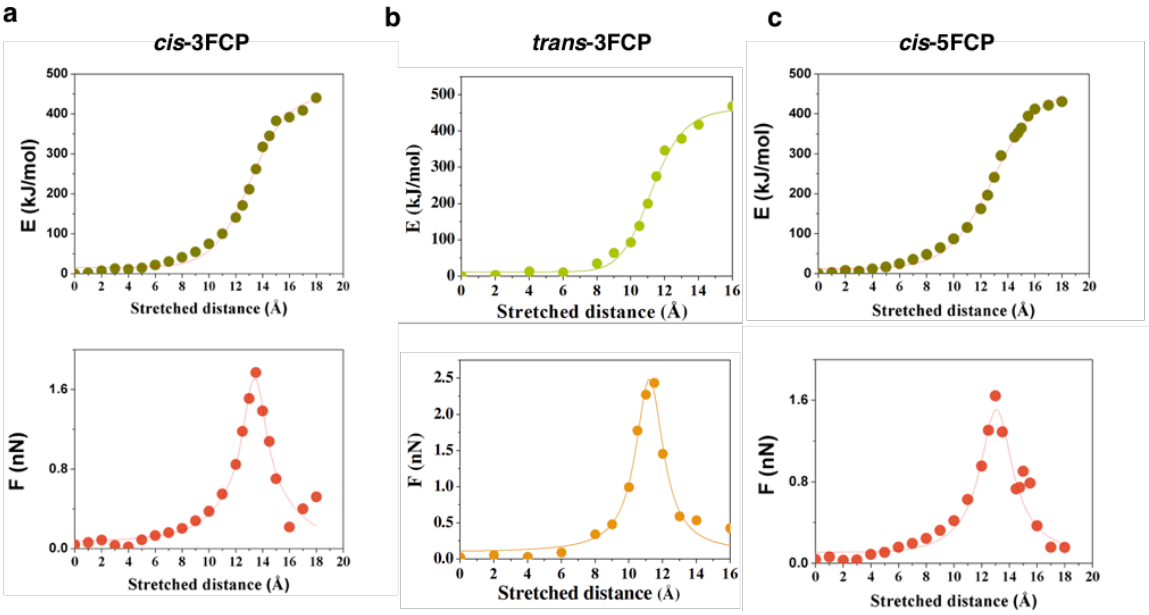

Figure S18. CoGEF potential and force as a function of stretched distance for *cis*-3FCP (a), *trans*-3FCP (b) and *cis*-5FCP (c) model compounds. The stretched distance defined as 0 Å when no stress is applied.

To further examine the effect of shearing versus peeling on ferrocene, we fixed the side chain angle of a ferrocene monomer to 0° so two Cp ligands were aligned in an eclipsed geometry, which will effectively drive the ferrocene to go down the peeling pathway. After the ferrocene dissociates, the fix applied on the side chains was removed. Similarly, CoGEF calculations were performed to obtain the equilibrium structure at each step as end-to-end distance is increased. We then compared the results to a ferrocene that undergoes shearing pathway as reported before.[5] As shown in Figure S19, the energy increases over a longer reaction coordinate for peeling than shearing. One consequence of that is the maximum force on the potential energy surface, which suggests an upper limit for ferrocene dissociation

force, is much less for peeling (1.1 nN) than shearing (3.1 nN). Because the force is applied over a larger distance, more energy is contributed through work to the reaction, which substantially lowers the force-coupled activation energy for the peeling pathway. The energy maximum, suggesting an upper limit of activation energy, for ferrocene dissociation through the peeling pathway is only 65 kcal/mol, which is substantially lower than the shearing pathway (87 kcal/mol, Table S17). These results suggest that a change in dissociation mechanism from shearing to peeling could lead to enhanced mechanochemical reactivity and is consistent with our observations from sonochemistry[5] and SMFS experiments. Interestingly, the energy maximum for *cis*-3FCP is higher than ferrocene that goes down the peeling pathway even if their reaction pathways and thermal stabilities are very similar. This can probably be attributed to the increased energy due to the distortion of bond angles between the *ansa*-bridge and Cp ligands when being stretched. Two pieces of evidence could support this: The Cp-Cp dihedral angle change is smaller for *cis*-3FCP compared to ferrocene under the same strain (Figure S20); H-H distance on C_1 and $C_{1'}$ for ferrocene decreases with stretching while the C_6-C_8 distance of *cis*-3FCP remains almost constant (Figure S21).

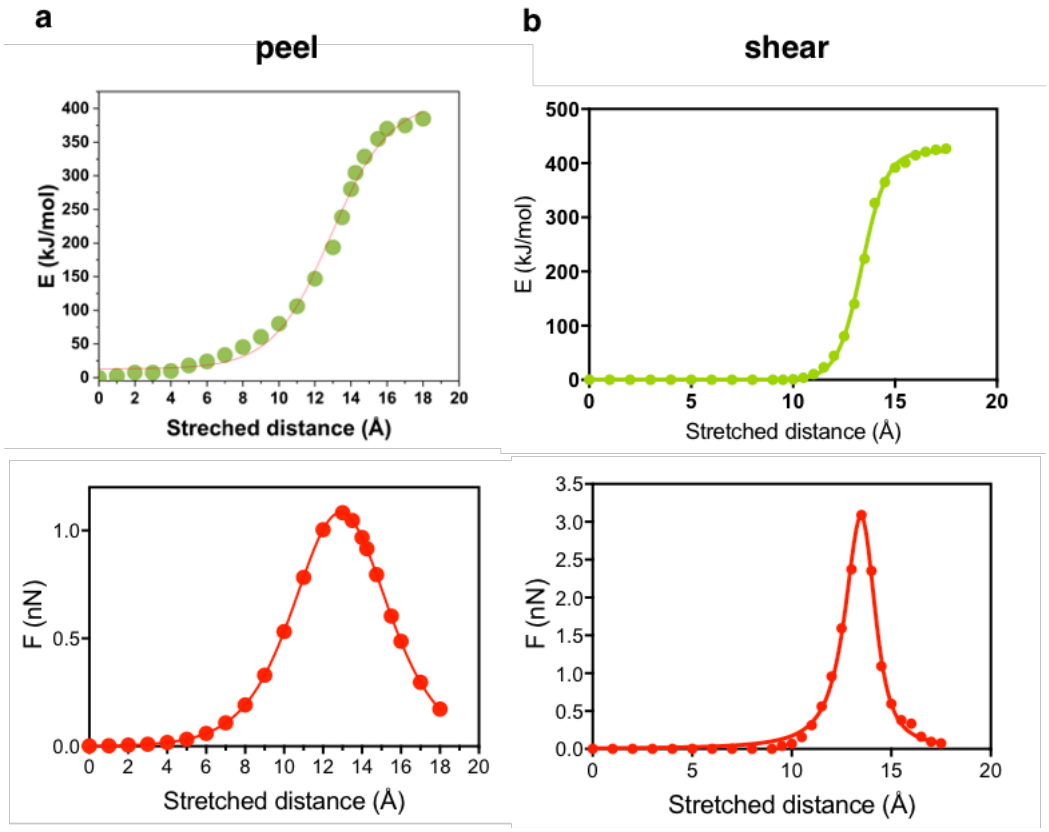

Figure S19. CoGEF potential and force as a function of stretched distance for ferrocene model compound that undergoes peeling (a) and shearing (b) pathways. The stretched distance defined as 0 Å when no stress is applied.

Table S17. Summary of energy maximum (calculated by energy at breaking point) for ferrocene and

ferrocenophanes under different pathways

Compound	Pathway	Energy Maximum (kcal/mol)
Ferrocene	Peel	65
Ferrocene	Shear	87
cis-3FCP	Peel	80
trans-3FCP	Peel + Shear	83
cis-5FCP	Peel	82

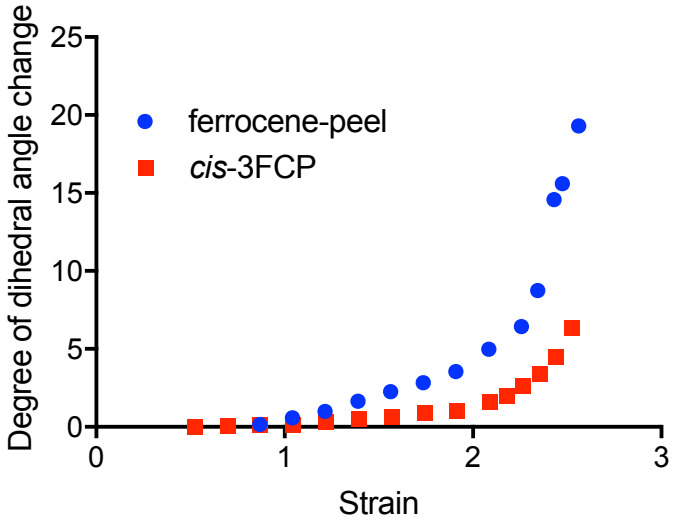

Figure S20. Degree of dihedral angle change (defined as Cp-Cp dihedral angle change over initial angle) under different strain (defined as end-to-end distance change over initial distance).

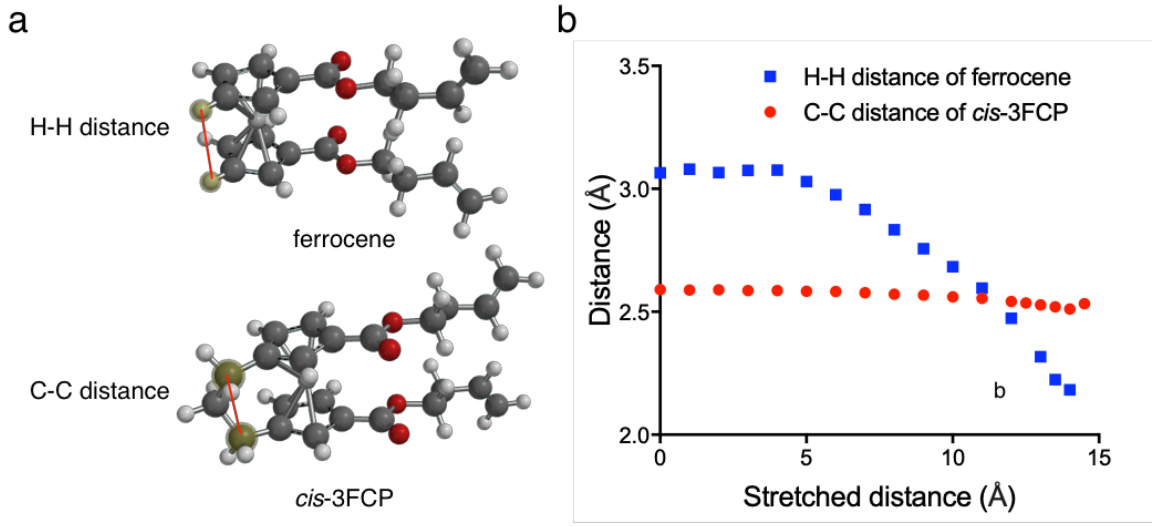

Figure S21. (a) Illustration of the measurement of C-C distance for *cis*-3FCP and H-H distance for ferrocene; (b) Distance change with stretched distance.

14. Measure of Cp plane-plane dihedral angle and angle between side chains

14.1 Measure of Cp plane-plane dihedral angle

The measurements were done in Mercury. The equilibrium geometry is obtained from DFT optimization and imported into Mercury. Two planes were created using the 5 carbon atoms of the

cyclopentadiene ring. Then the dihedral angles of the two planes were read automatically.

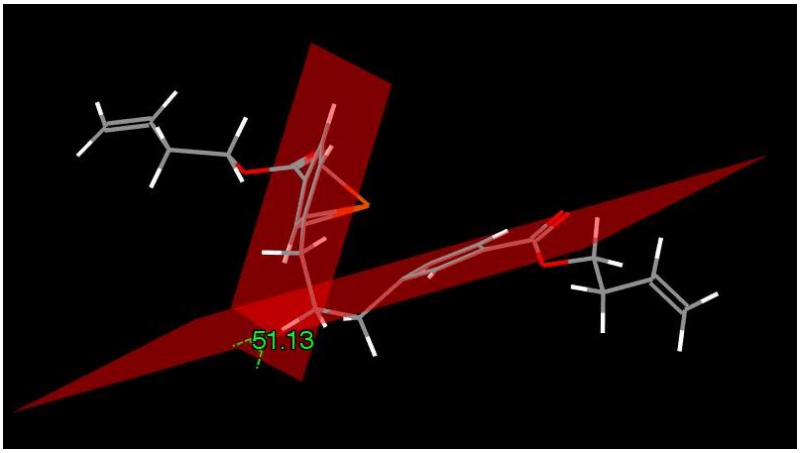

Figure S22. Example of measurement of Cp plane-plane dihedral angles for *trans*-3FCP at breaking point (displacement = 12 Å).

14.2 Measurement of angle between side chains

The measurements were done in Gaussian 09. The equilibrium structure is obtained from DFT optimization. 4 atoms from the two side chains (highlighted in Figure S23) were selected following this order: 21, 2, 7, 18. The dihedral angles were read automatically from the software.

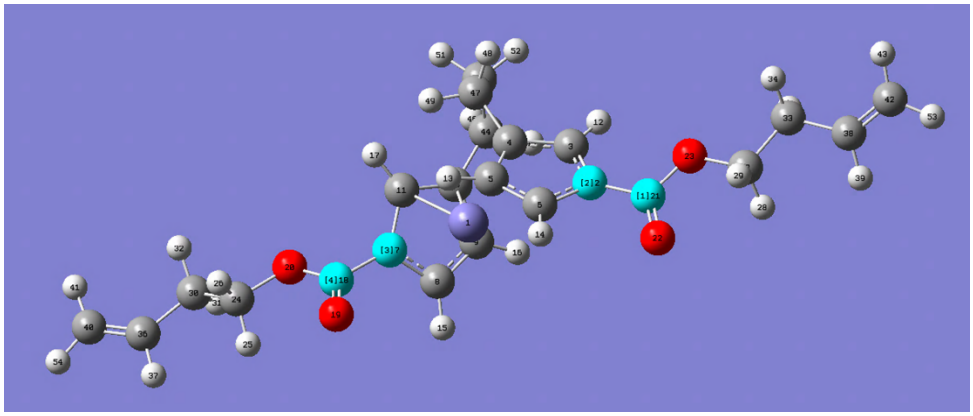

Figure S23. Example of measurement of side chain dihedral angles for *trans*-3FCP at breaking point (displacement = 12 Å).

15. NMR spectra

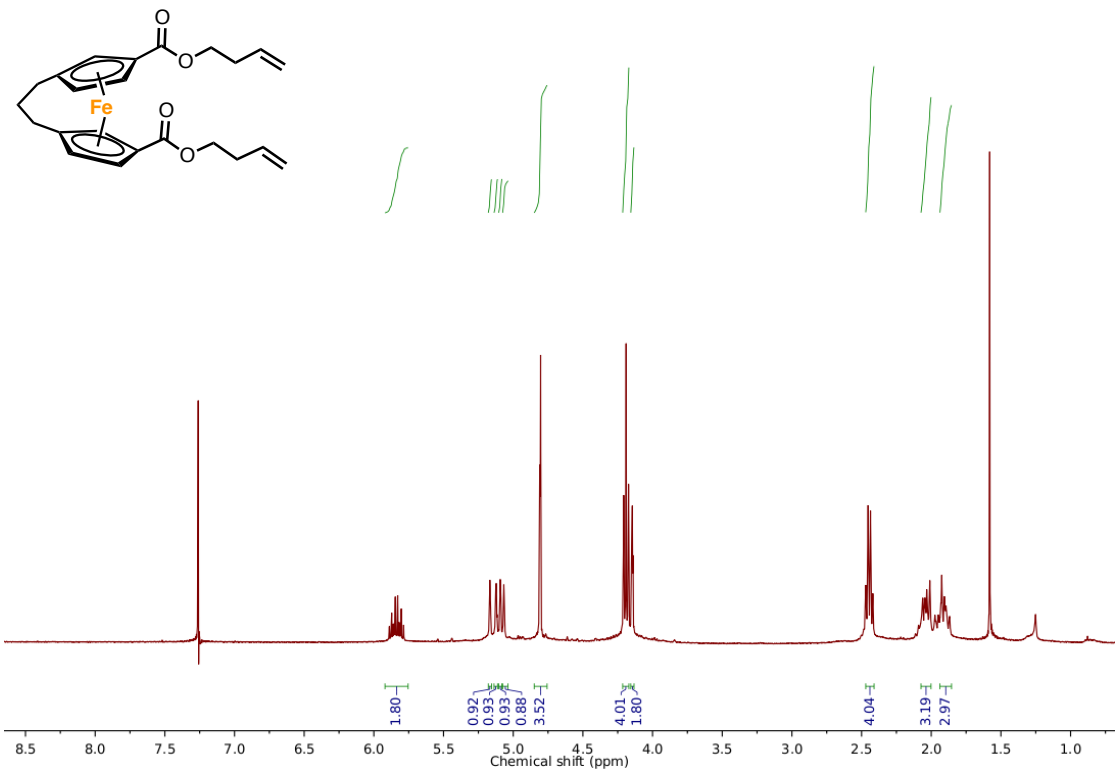

Figure S24. ^{1}H NMR spectrum of **1** in $CDCl_3$.

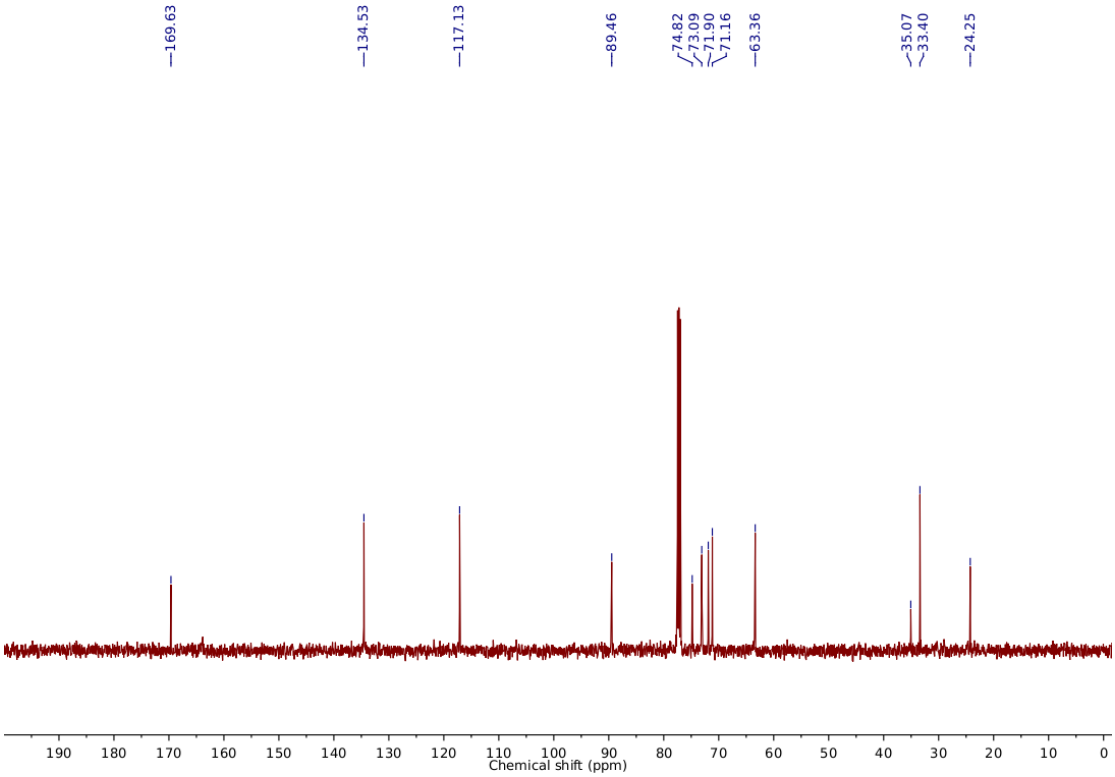

Figure S25. ^{13}C NMR spectrum of **1** in $CDCl_3$.

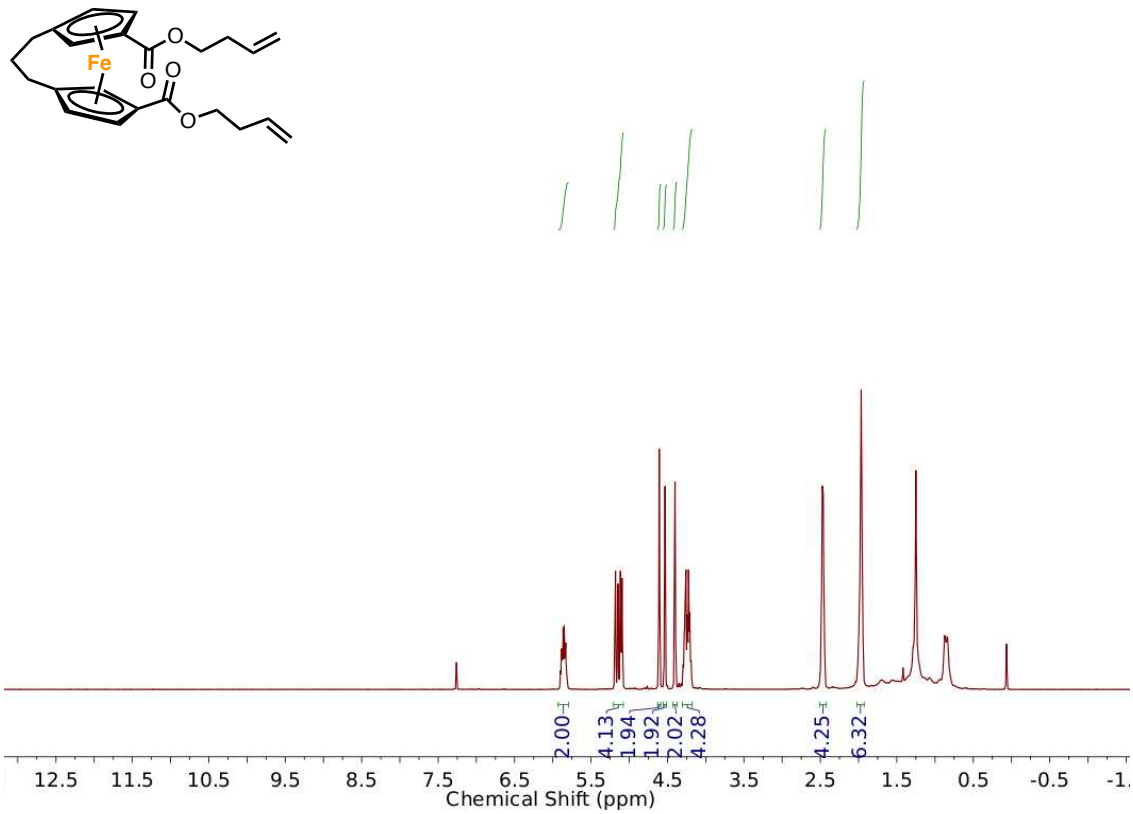

Figure S26. ^{1}H NMR spectrum of **2** in $CDCl_3$.

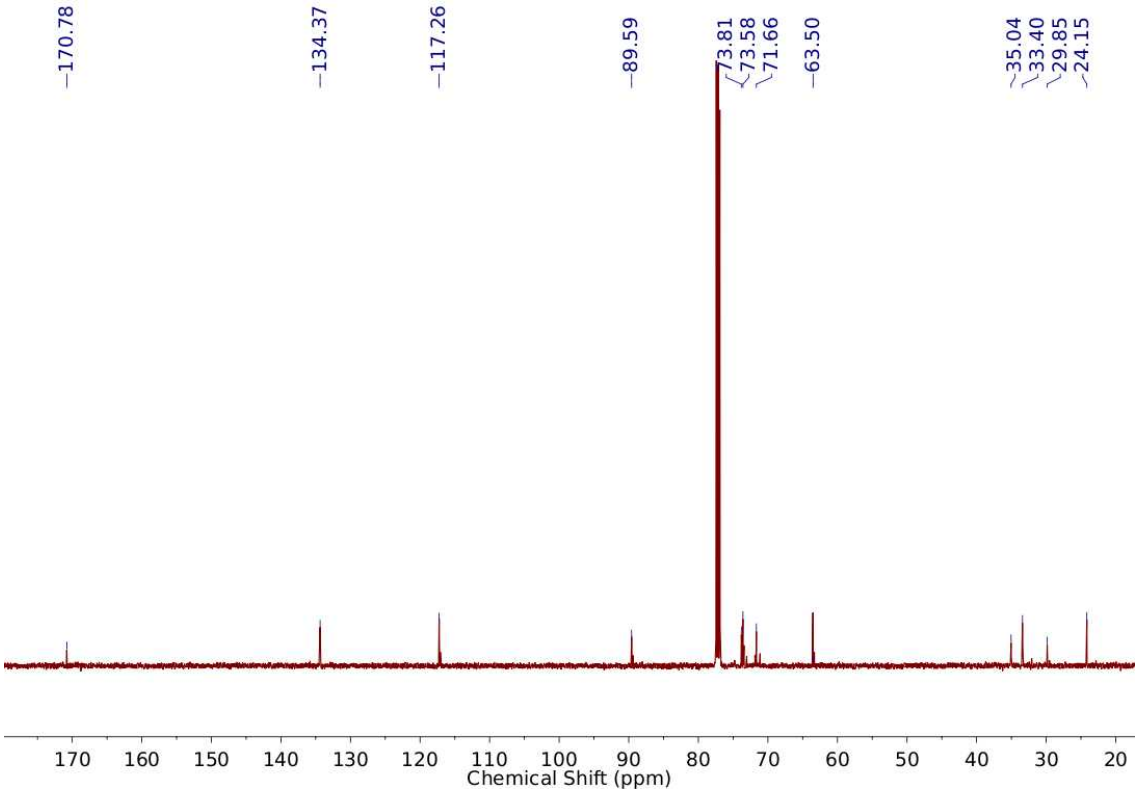

Figure S27. ^{13}C NMR spectrum of **2** in $CDCl_3$.

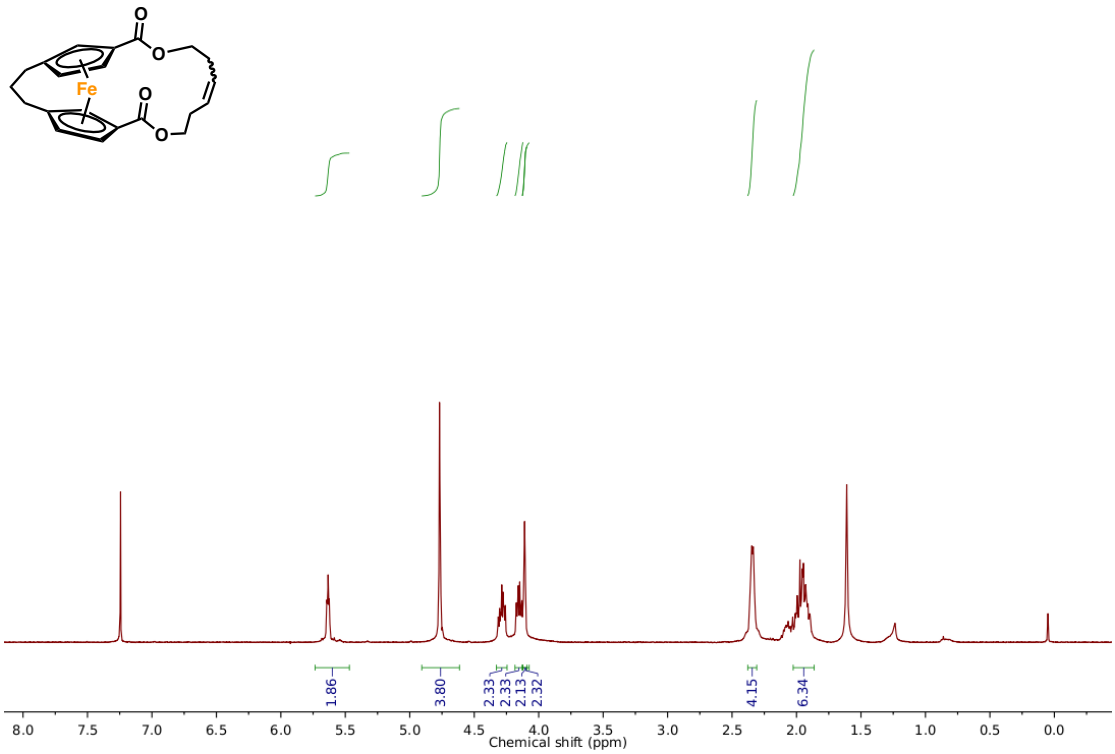

Figure S28. ^{1}H NMR spectrum of **3** in $CDCl_3$.

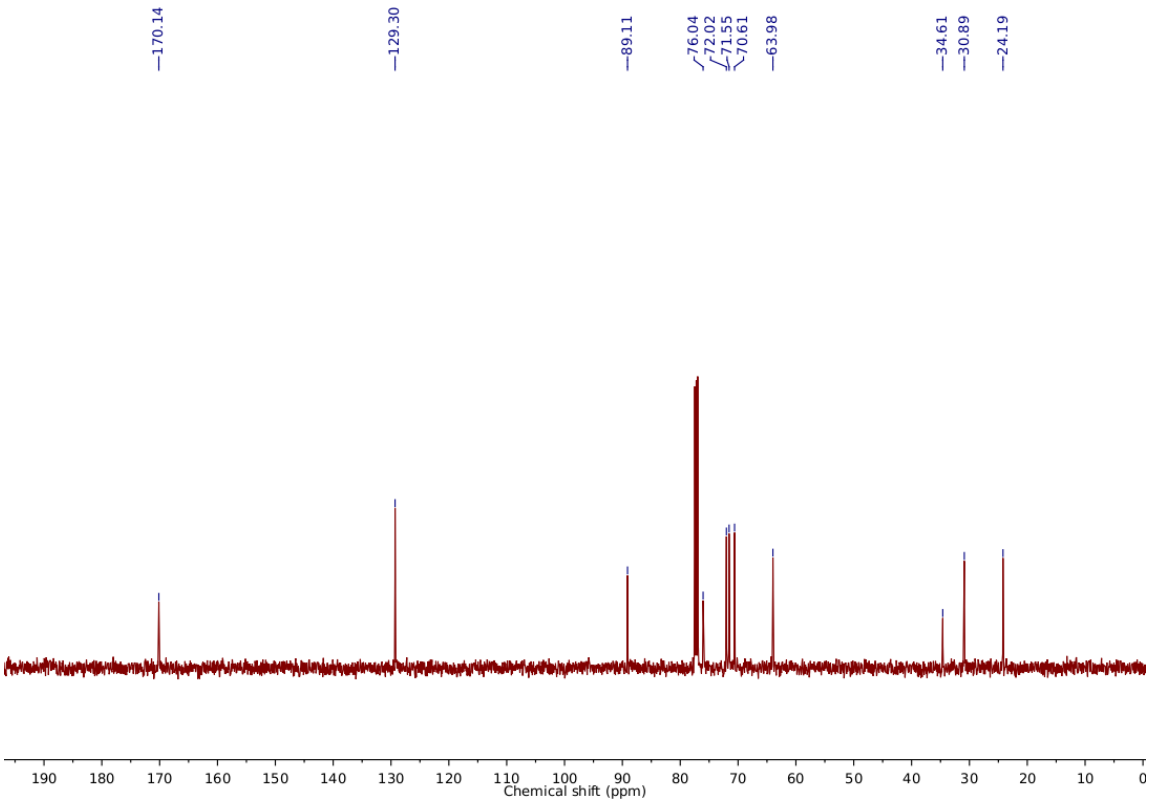

Figure S29. ^{13}C NMR spectrum of **3** in $CDCl_3$.

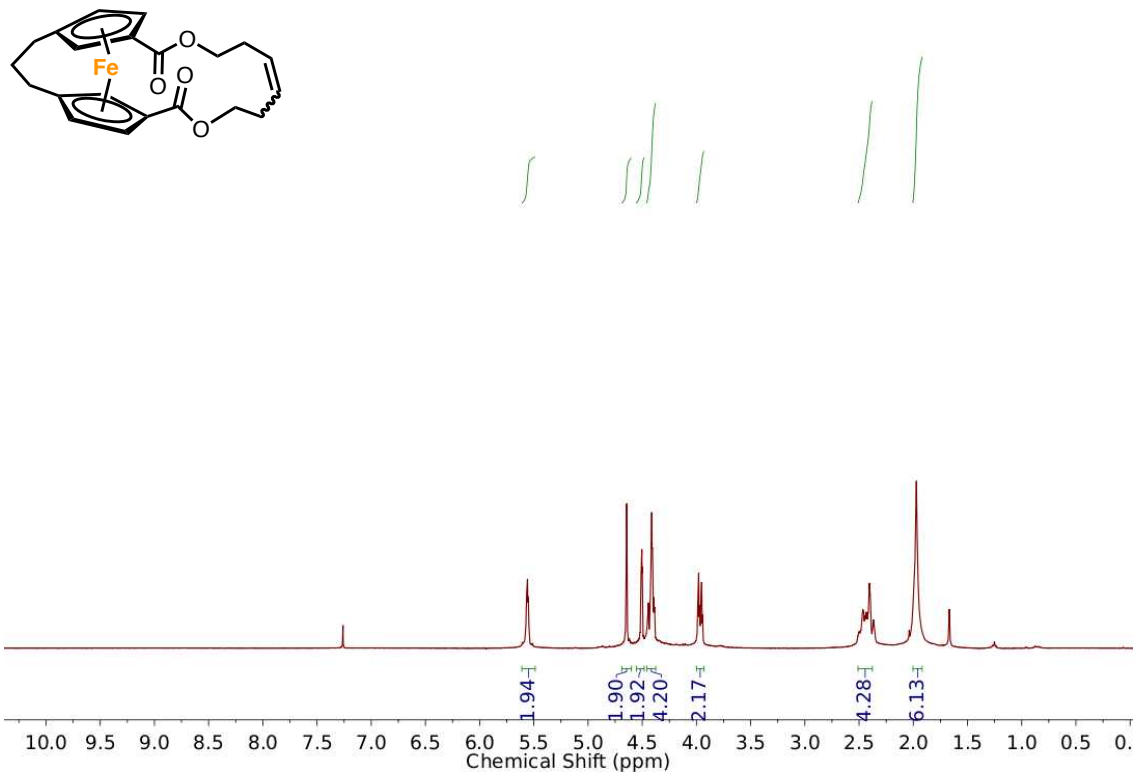

Figure S30. ^{1}H NMR spectrum of **4** in $CDCl_3$.

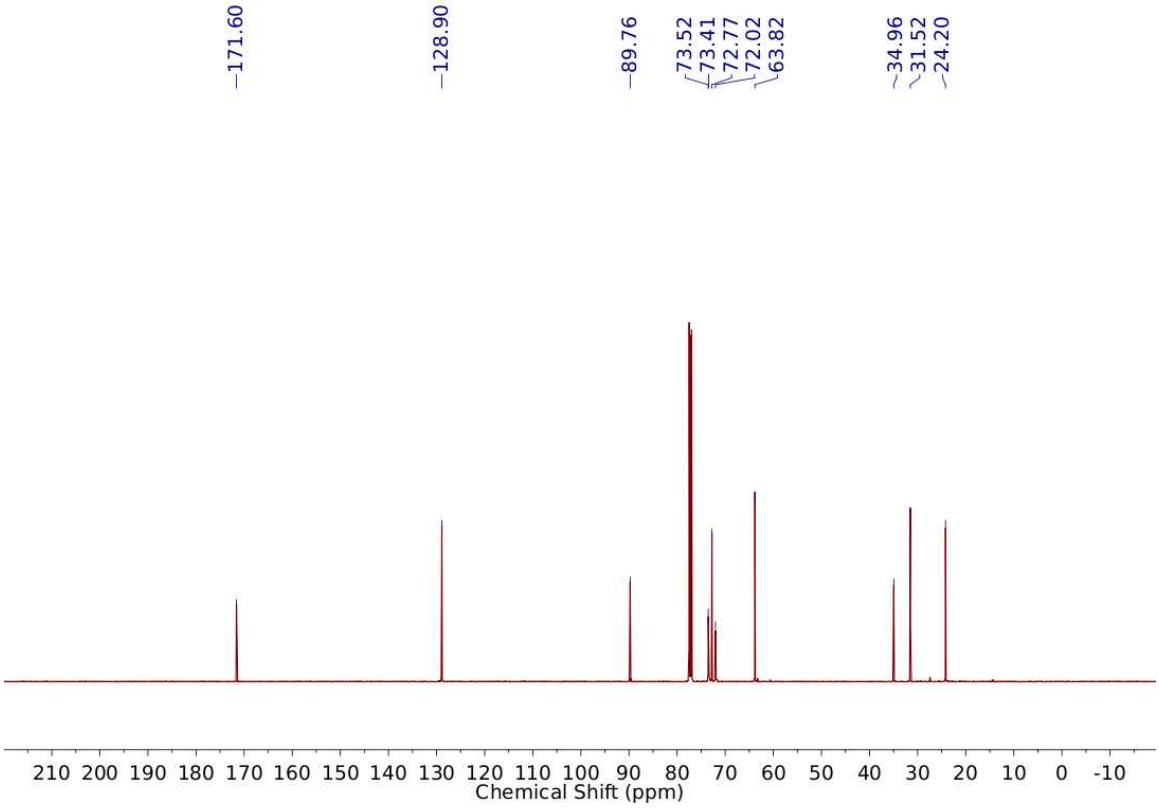

Figure S31. ^{13}C NMR spectrum of **4** in $CDCl_3$.

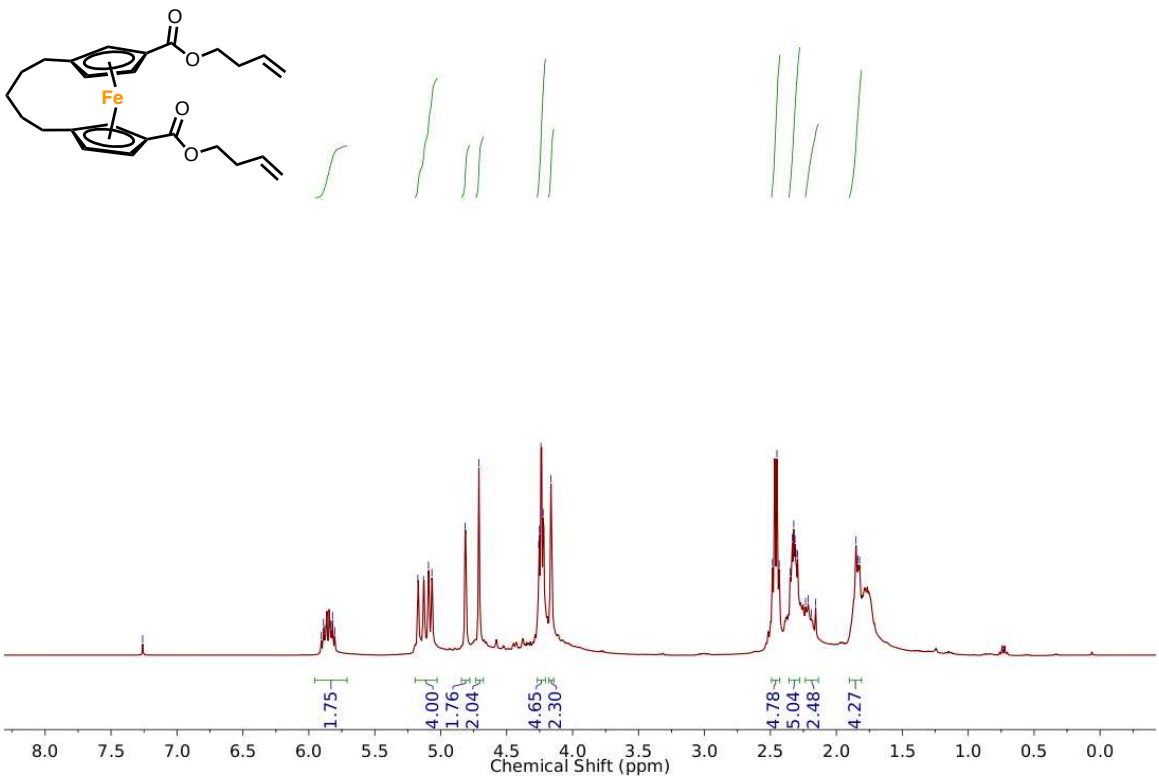

Figure S32. ^{1}H NMR spectrum of **5** in $CDCl_3$.

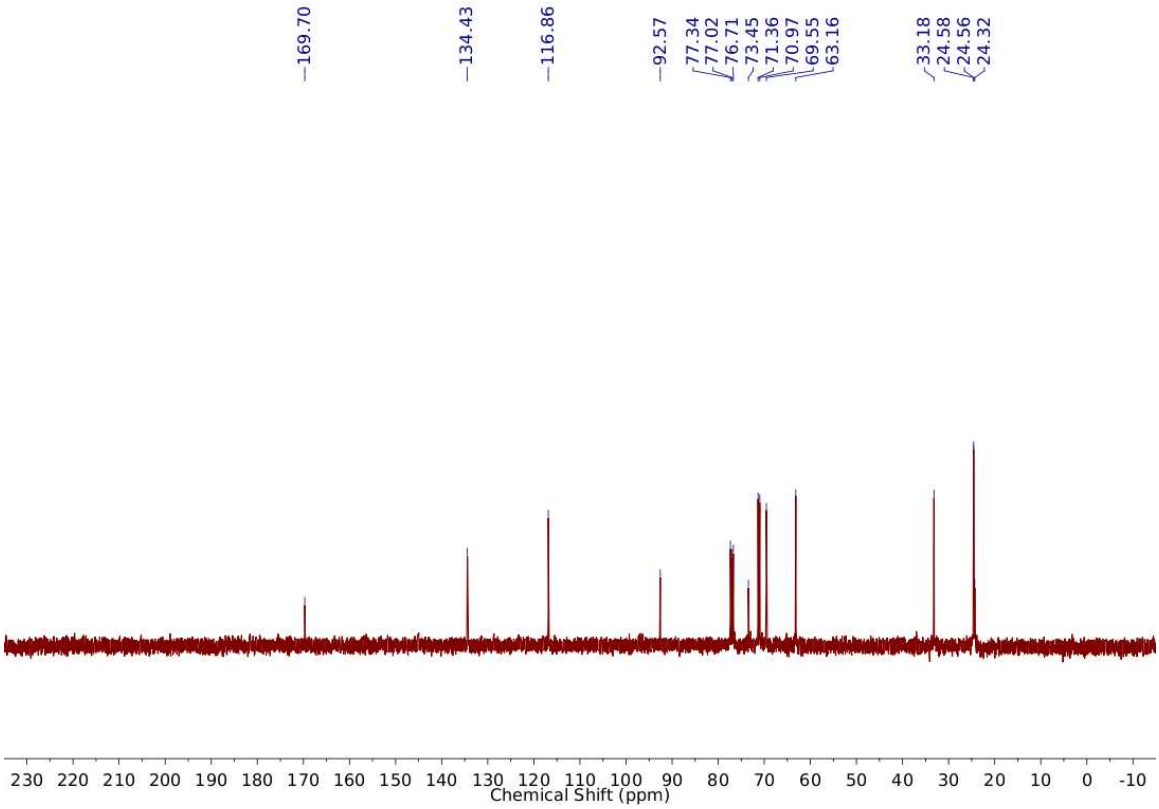

Figure S33. ^{13}C NMR spectrum of **5** in $CDCl_3$.

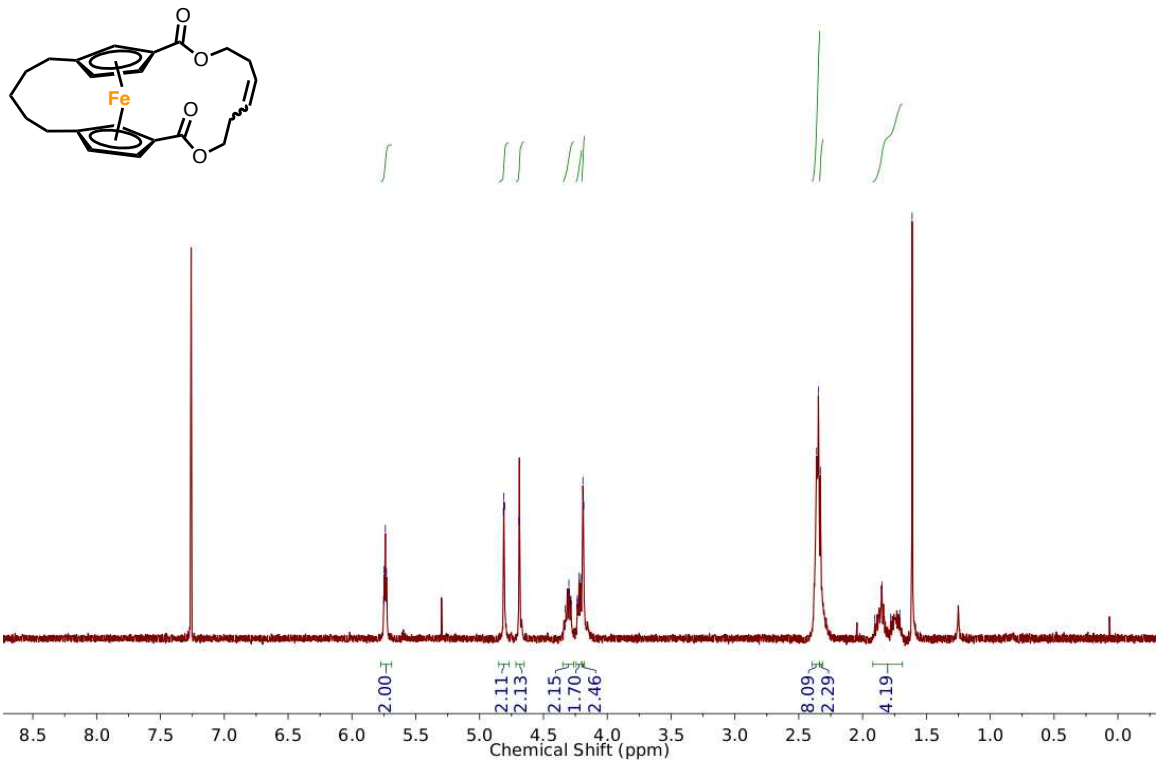

Figure S34. ^{1}H NMR spectrum of **6** in $CDCl_3$.

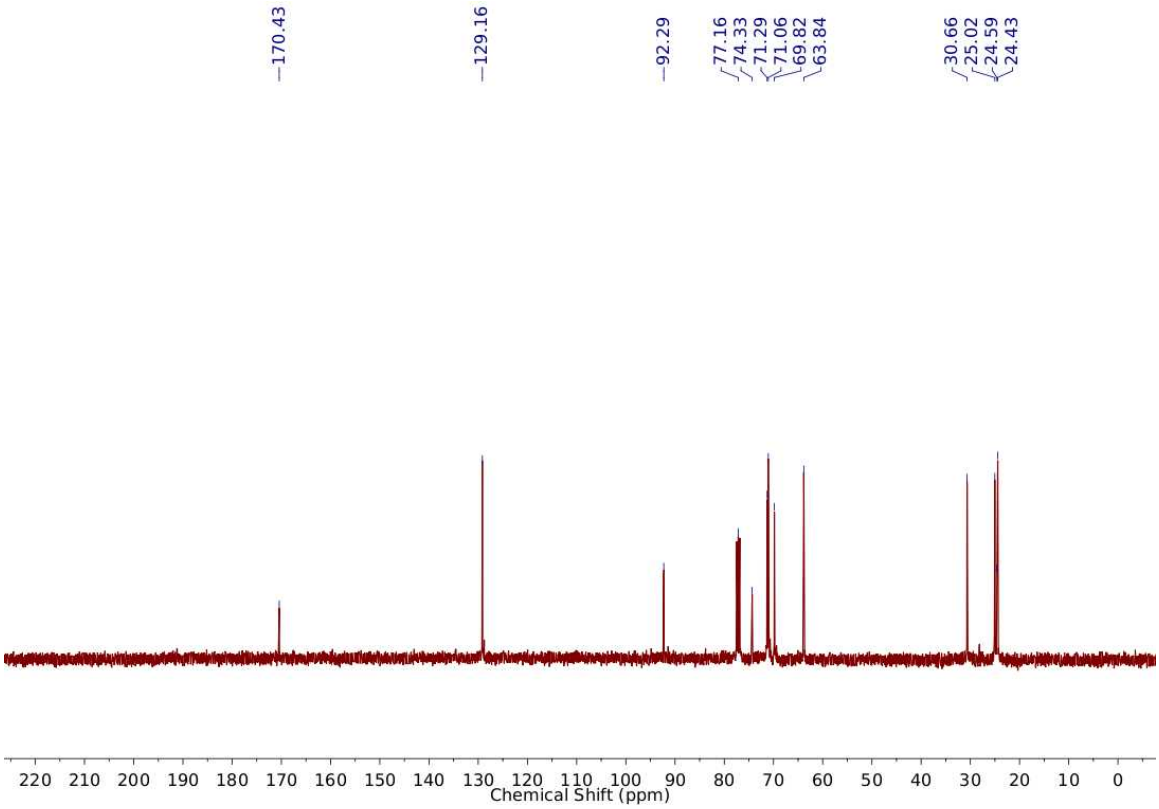

Figure S35. ^{13}C NMR spectrum of **6** in $CDCl_3$.

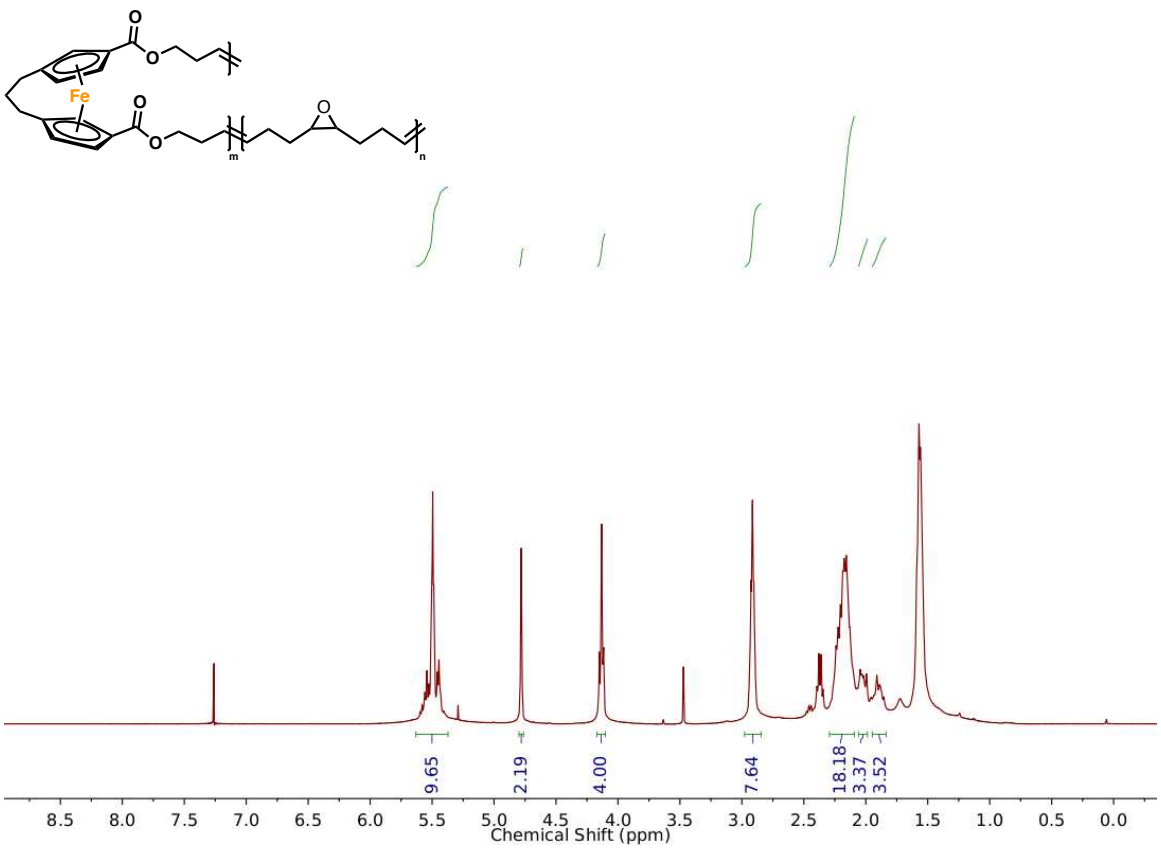

Figure S36. ^{1}H NMR spectrum of **7** (16% incorporation) in $CDCl_3$.

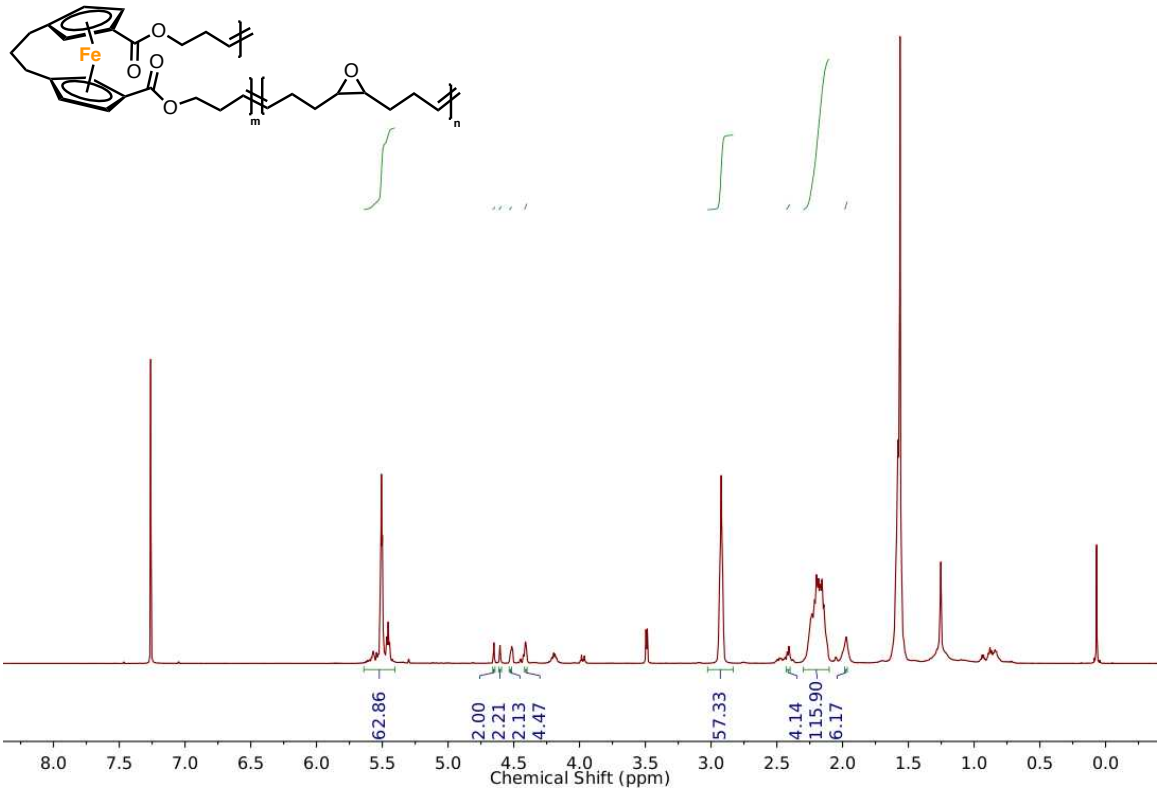

Figure S37. ^{1}H NMR spectrum of **8** (6% incorporation) in $CDCl_3$.

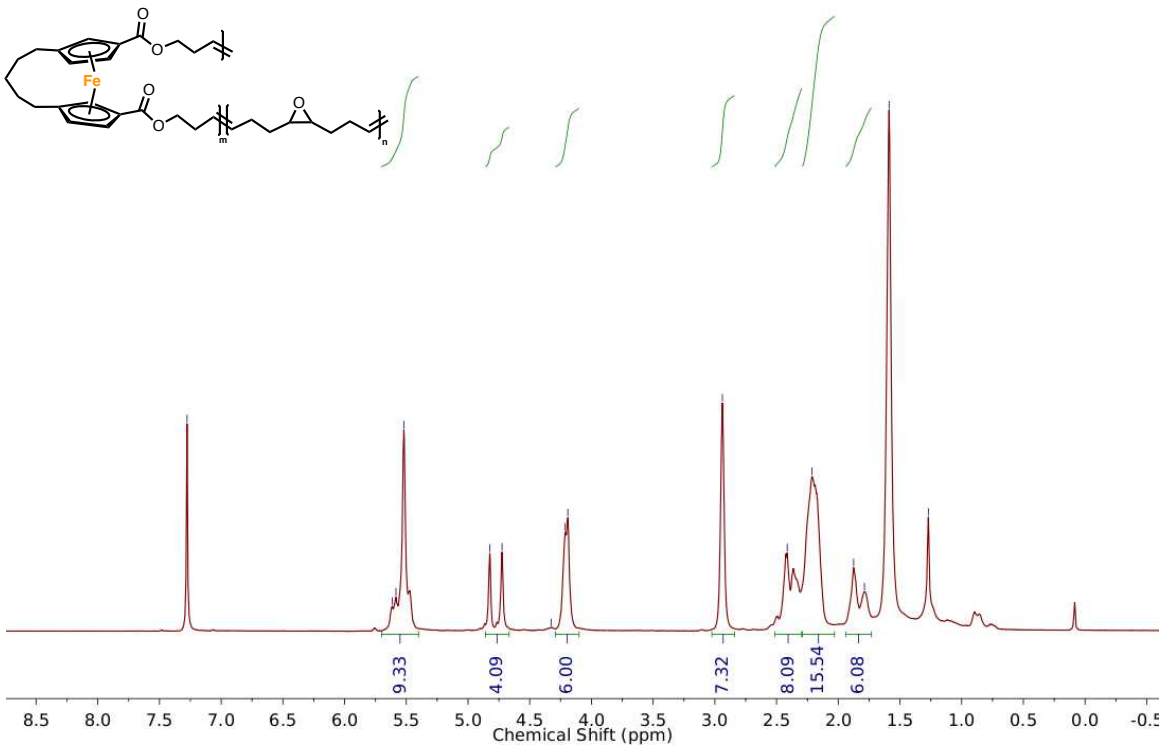

Figure S38. ^{1}H NMR spectrum of **9** (15% incorporation) in $CDCl_3$.

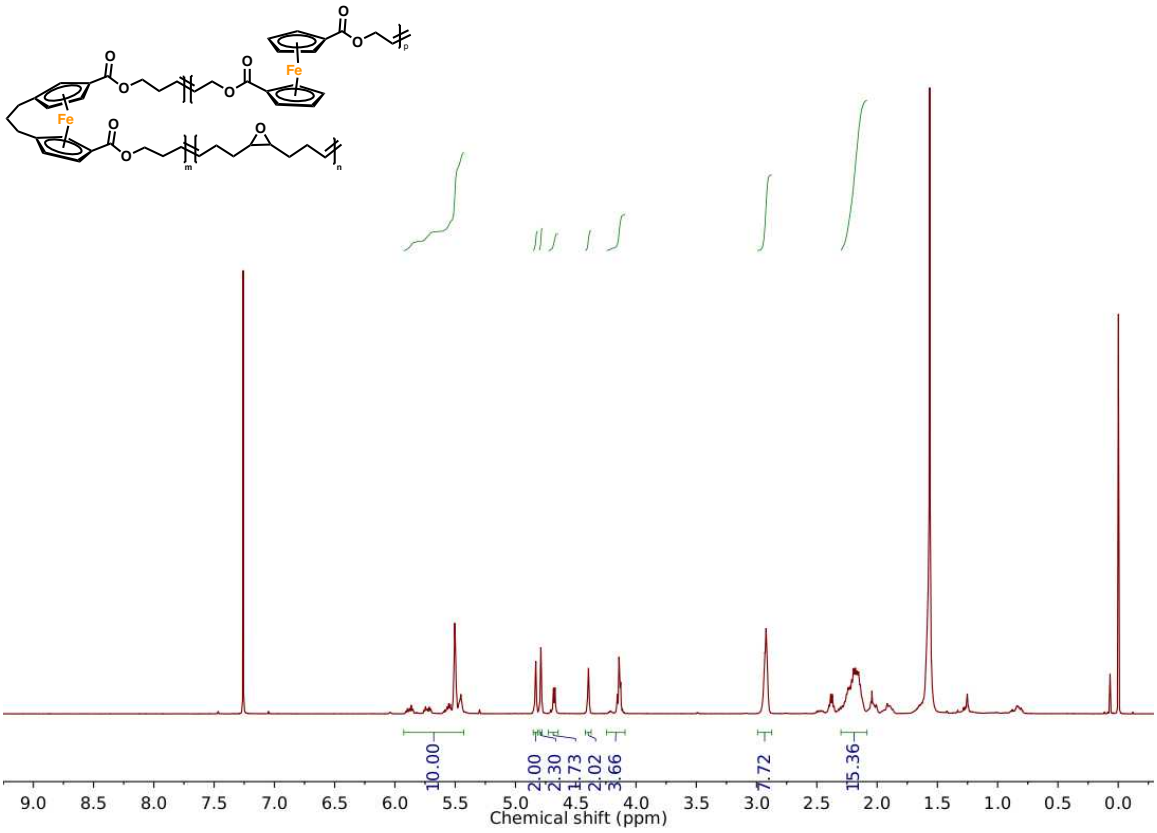

Figure S39. ^{1}H NMR spectrum of **10** (11% FC, 28% *cis*-3FCP) in $CDCl_3$.

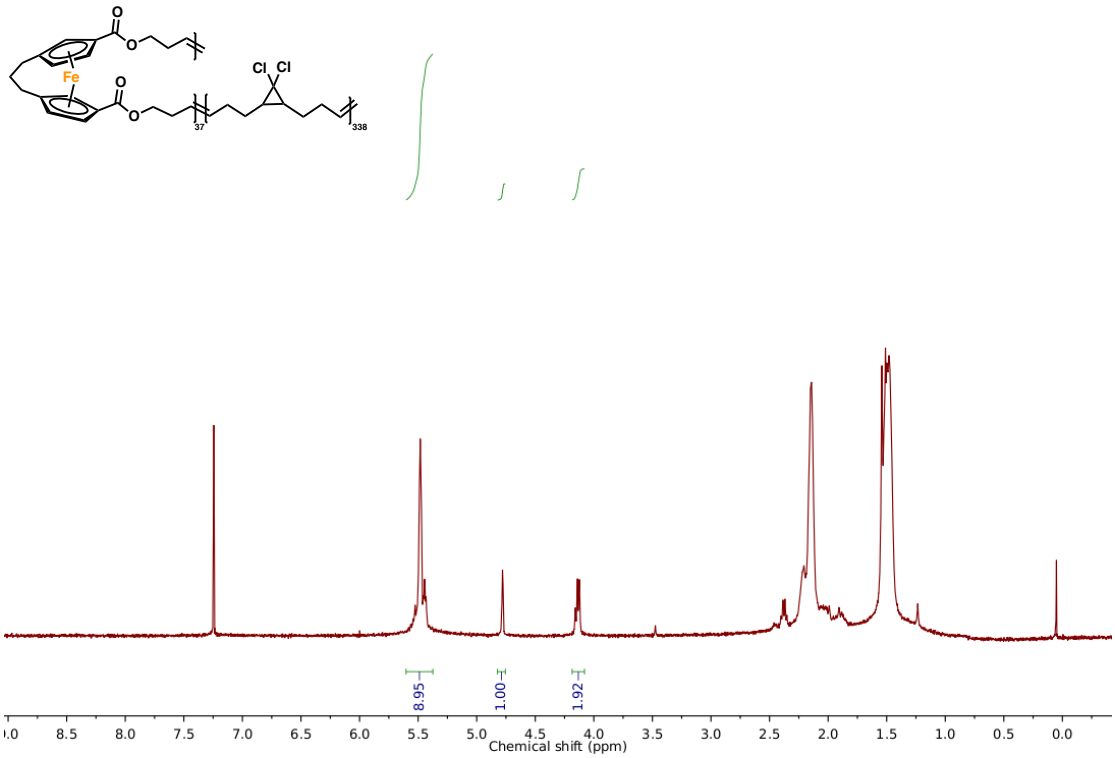

Figure S40. ^{1}H NMR spectrum of **11 (**10% incorporation**)** in $CDCl_3$.

16. References:

1 Turbitt, T. & Watts, W. Bridged ferrocenes: XII. The synthesis of [3] ferrocenophan-1-one from ferrocene by a novel one-step annelation reaction. *J. Organomet. Chem.* **46**, 109-117 (1972).

2 Hisatome, M. & Hillman, M. Bridged ferrocenes: VII. Synthesis of di-and tri-bridged ferrocenes with pentamethylne chains. *J. Organomet. Chem.* **212**, 217-231 (1981).

3 Kouznetsova, T. B., Wang, J. & Craig, S. L. Combined Constant-Force and Constant-Velocity Single-Molecule Force Spectroscopy of the Conrotatory Ring Opening Reaction of Benzocyclobutene. *ChemPhysChem* **18**, 1486-1489 (2017).

4 Gossweiler, G. R. *et al.* Mechanochemical Activation of Covalent Bonds in Polymers with Full and Repeatable Macroscopic Shape Recovery. *ACS Macro Lett.* **3**, 216-219 (2014).

5 Sha, Y. *et al.* Quantitative and Mechanistic Mechanochemistry in Ferrocene Dissociation. *ACS Macro Lett.* **7**, 1174-1179 (2018).

6 Shannahan, L. *et al.* A Mechanochemistry-Based Technique For Early Material Damage Detection In High Strain Rate Processes. (ARMY RESEARCH LAB ABERDEEN PROVING GROUND MD ABERDEEN PROVING GROUND United States, 2019).

7 Hillman, M., Matyevich, L., Fujita, E., Jagwani, U. & McGowan, J. Bridged ferrocenes. 9. Lithiation and subsequent reactions of 1, 1'-trimethyleneferrocene. *Organometallics* **1**, 1226-1229 (1982).

8 Gossweiler, G. R., Kouznetsova, T. B. & Craig, S. L. Force-rate characterization of two spiropyran-based molecular force probes. *J. Am. Chem. Soc.* **137**, 6148-6151 (2015).

9 Serpe, M. J. *et al.* A simple and practical spreadsheet-based method to extract single-molecule dissociation kinetics from variable loading-rate force spectroscopy data. *J. Phys. Chem. C* **112**, 19163-19167 (2008).

10 E. S. Domalski, E. D. H., J. A. Martinho Simoes. (National Institute of Standards and Technology (NIST)).

11 Nelson, J. M., Rengel, H. & Manners, I. Ring-opening polymerization of [2] ferrocenophanes with a hydrocarbon bridge: synthesis of poly (ferrocenylethylenes). *J. Am. Chem. Soc.* **115**, 7035-7036 (1993).

12 Siemeling, U., Krallmann, R., Jutzi, P., Neumann, B. & Stammler, H.-G. [3] Ferrocenophanes with a tetramethyldisiloxane bridge: Synthesis and molecular structure. *Monatsh. Chem.* **125**, 579-586 (1994).

13 Musgrave, R. A. *et al.* Main-chain metallopolymers at the static–dynamic boundary based on nickelocene. *Nature Chem.* **9**, 743 (2017).

14 Gilroy, J. B. *et al.* An iron-cyclopentadienyl bond cleavage mechanism for the thermal ring-opening polymerization of dicarba [2] ferrocenophanes. *Chem. Sci.* **3**, 830-841 (2012).

15 Nelson, J. M. *et al.* Thermal Ring-Opening Polymerization of Hydrocarbon-Bridged [2] Ferrocenophanes: Synthesis and Properties of Poly (ferrocenylethylene) s and Their Charge-Transfer Polymer Salts with Tetracyanoethylene. *Chem. Eur. J.* **3**, 573-584 (1997).